

## First-principles calculations of the structure of MgSiO<sub>3</sub> melt at high temperature and high pressure

MATSUI, Masanori<sup>1\*</sup>

<sup>1</sup>School of Sci., Univ. of Hyogo

Crystals and melts with MgSiO<sub>3</sub> composition are important constituents of the Earth's lower crust and mantle. Therefore an accurate knowledge of their structural and elastic properties at high temperatures and high pressures is crucial to investigate the chemical and physical structures, and the conditions of formation and evolution of the Earth. However, reliable experimental data under geophysically relevant conditions are generally lacking for MgSiO<sub>3</sub> melt, mainly due to the difficulty in obtaining such data at the combined high temperature and high pressure found in the Earth's interior. Here we use the first-principles molecular dynamics (FPMD) method to study the structures and elastic properties of MgSiO<sub>3</sub> melt at high temperatures and high pressures.

All calculations were performed with the Vienna Ab Initio Simulation Package VASP (Kresse and Furthmuller, 1996). The projector-augmented wave (PAW) method was used in the local density approximation (LDA) for the exchange-correlation functional (Blochl, 1994; Kresse and Joubert, 1999). FPMD calculations were carried out in the canonical ensemble (constant temperature  $T$ , constant volume  $V$ , and constant number of atoms  $N$  in the system) using cubic basic cells.  $N$  was taken to be 160 (32 MgSiO<sub>3</sub>) throughout this study. After annealing the system sufficiently at 4000 K, and then 3000 K, we fixed  $V$  at 38.54 cm<sup>3</sup>/mol and  $T$  at 2000 K to calculate the interference function  $S(Q)$ , where  $Q$  is the length of scattering vector, and the radial distribution function (RDF) for each atom pair. We found FPMD calculated  $S(Q)$  compares reasonably well with the observed data from X-ray analyses at 1973 K by Waseda and Toguri(1990). The FPMD predicted average nearest neighbor bond distances  $r(ij)$ , and coordination numbers  $n(ij)$  between atoms  $i$  and  $j$  are also compared well with the data by Waseda and Toguri(1990), except the  $r(\text{MgO})$  distance, in which the FPMD value of 1.97 Å is much shorter than the value [2.12(1) Å] by the X-ray analyses. We further apply the FPMD technique to investigate the temperature and pressure dependencies of the structure of MgSiO<sub>3</sub> melt.

Keywords: MgSiO<sub>3</sub> melt, high temperature, high pressure, first-principles calculation

## Forsterite-MgSiO<sub>3</sub> liquid interface : molecular dynamics perspective

NORITAKE, Fumiya<sup>1\*</sup> ; KAWAMURA, Katsuyuki<sup>1</sup>

<sup>1</sup>Okayama University

Knowledge about the viscosity and permeability of partial molten rocks is important to understand the thermal history of the Earth and volcanisms. For understanding those obtained by experiments and estimating the physical properties at extreme conditions those are difficult to reproduce in laboratory experiments, the knowledge about structure and properties of silicate crystal-liquid interfaces is necessary. The properties of melt as sandwiched thin films are considered as being different with ones in bulk melts by the effect of crystal surface. For instance, lateral self-diffusivity of water to crystal surfaces shows different from bulk one in the case of water-brucite surface (Sakuma et al. 2003), water-muscovite mica surface (Sakuma and Kawamura, 2009). The dynamic property anomalies on solid - liquid surfaces affect properties of bulk rock such as permeability (Ichikawa et al. 2001).

In this study, structure and properties of the forsterite-MgSiO<sub>3</sub> liquid interfaces are investigated by using molecular dynamics simulations. It is essential to know the structure and physical properties of forsterite-MgSiO<sub>3</sub> liquid interfaces since forsterite is the liquidus mineral of primordial magmas.

Molecular dynamics simulations were performed with NPT ensemble using MXDORTO code (Sakuma and Kawamura, 2009). The initial structure is a 21440 atom system in which a sheet of MgSiO<sub>3</sub> liquid consist of 8000 atoms (~5 nm) is sandwiched between (010) surfaces of forsterite(Pbnm) and 43440 atom system in which a sheet of MgSiO<sub>3</sub> liquid consist of 30000 atoms (~20 nm) is sandwiched between (010) surfaces of forsterite. Firstly we calculated equilibrated MgSiO<sub>3</sub> liquid film in vacuum starting with a randomly generated structure and randomly generated velocities of atoms through 0.5 ns (1,000,000 steps) at 1973 K and quench to 300 K. Secondly we calculated a bulk forsterite crystal with 13440 atoms (11\*5\*8 unit cells of forsterite(Pbnm)) starting with a given experimental crystal structure which was obtained by the experiment [5] and with randomly generated velocities of atoms and then cut along (010) surface. Finally we combined forsterite cut along (010) surface and MgSiO<sub>3</sub> liquid film. Under maintaining isobaric and isothermal conditions, we performed the relaxation of 0.5~1.5 ns. Then the statistical averages of the structure and physical properties were obtained from the velocities and coordinates of each atom in the simulations through 500 ps. The function of inter-atomic potential model was same as used in our previous work (Noritake et al. 2012).

By these simulations, characteristic structures in the forsterite-MgSiO<sub>3</sub> liquid interface are observed. The layered structure of alternated crystal surface, Si-rich and Mg-rich layers in the crystal-liquid interface was observed. The layered structure was formed by energy difference between Si-O semi-covalent bonds and Mg-O ionic bonds. Si-O-Si bridging and free oxygen atoms are excessively formed and in the near surface since the energy of Si-O bonding is much lower than that of Mg-O bonding. The difference of layered structure by thickness of MgSiO<sub>3</sub> liquid film might be caused by the difference of the degree of freedom of configuration in liquid film. The two-dimensional diffusivity of oxygen atoms is controlled by two factors. The one is the thickness of liquid film that decreases oxygen diffusivity with decreasing the film thickness because of decrease of degree of freedom of configuration in liquid film. The other is composition of sliced layer where oxygen diffusivity increases with increasing the Mg/Si ratio since Si-O bonding is much stronger than Mg-O ones.

Keywords: Interface, High-Temperature, Silicates, Molecular dynamics simulation

## Phase transitions in $\text{Zn}_2\text{SiO}_4$ : first-principles study

KANZAKI, Masami<sup>1\*</sup>

<sup>1</sup>Inst. Study Earth's Interior, Okayama University

Recent experimental study (Liu et al., *PCM*, 40, 467, 2013) suggested that high-pressure phases of III and IV in  $\text{Zn}_2\text{SiO}_4$  could be retrograde phases transformed during decompression. In order to check stabilities of these phases under pressure, and to find original high-pressure phases, density functional theory total energy calculations of 12 phases at 0 K have been conducted.

Three pressure-induced "phase transitions" during structural optimization were observed: phase II to spinel structure, phase III to a new high-pressure phase, and phase IV to  $\text{Na}_2\text{SO}_4$  III-type structure. Phase III, having tetrahedral olivine structure, exhibited extraordinary high compressibility, which is due to large volume reductions in vacant octahedral sites corresponding M1 and M2 sites in olivine structure. Calculated enthalpies of the phases at 0 K confirmed that phase III and IV are not stable at any pressure. It also suggested that  $\text{Na}_2\text{SO}_4$  III and II phases will be stable phases replacing phase III and IV, respectively.

Keywords:  $\text{Zn}_2\text{SiO}_4$ , phase transition, high pressure phase, first-principles, transition mechanism

## A new high pressure phase of Fe<sub>2</sub>SiO<sub>4</sub> and the relationship between spin and structural transitions

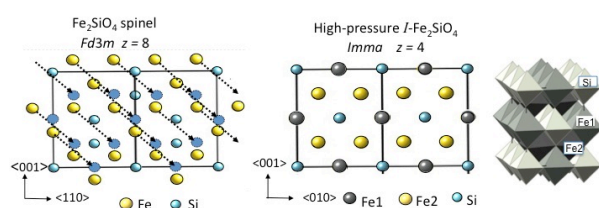
YAMANAKA, Takamitsu<sup>1\*</sup>; KYONO, Atsushi<sup>2</sup>; NAKAMOTO, Yuki<sup>3</sup>; KHARLAMOVA, Svetlana<sup>1</sup>; STRUZKIN, Viktor<sup>1</sup>; MAO, Ho-kwang<sup>1</sup>; HEMLY, Russell<sup>1</sup>

<sup>1</sup>Carnegie Institution of Washington Geophysical Laboratory, <sup>2</sup>Division of Earth Evolution Sciences, Life and Environment Sciences, University of Tsukuba, <sup>3</sup>Center for Quantum Science and Technology Under Extreme Conditions, Osaka University

A structural change in Fe<sub>2</sub>SiO<sub>4</sub> spinel (ringwoodite) has been found by synchrotron powder diffraction study and the structure of a new high-pressure phase was determined by Monte-Carlo simulation method and Rietveld profile fitting of x-ray diffraction data up to 64 GPa at ambient temperature. A transition from the cubic spinel structure to a body centered orthorhombic phase (I-Fe<sub>2</sub>SiO<sub>4</sub>) with space group *Imma* and Z=4 was observed at approximately 34 GPa. The structure of I-Fe<sub>2</sub>SiO<sub>4</sub> has two crystallographically independent FeO<sub>6</sub> octahedra. Iron resides in two different sites of six-fold coordination: Fe1 and Fe2, which are arranged in layers parallel to (101) and (011), and very similar to the layers of FeO<sub>6</sub> octahedra in the spinel structure. Silicon is located in the six-fold coordination in I-Fe<sub>2</sub>SiO<sub>4</sub>. The transformation to the new high-pressure phase is reversible under decompression at ambient temperature. A martensitic transformation of each slab of the spinel structure with transition vector  $\langle 1/8 \ 1/8 \ 1/8 \rangle$  generates the I-Fe<sub>2</sub>SiO<sub>4</sub> structure. Laser heating of I-Fe<sub>2</sub>SiO<sub>4</sub> at 1500 K results in a decomposition of the material to rhombohedral FeO and SiO<sub>2</sub> stishovite.

Fe K beta x-ray emission measurements at high pressure up to 65GPa show that the transition from a high spin (HS) to an intermediate spin (IS) state begins at 17 GPa in the spinel phase. The IS electron spin state is gradually enhanced with pressure. The Fe<sup>2+</sup> ion at the octahedral site changes the iron radius under compression from 0.78 Å at the high-spin state to 0.61 Å at the low spin, which results in the changes of the lattice parameter and the deformation of the octahedra of the spinel structure. The compression curve of the lattice parameter of the spinel is discontinuous at approximately 20 GPa. The spin transition induces an isostructural change.

Keywords: Fe<sub>2</sub>SiO<sub>4</sub> spinel, new high-pressure phase, spin transition, X-ray emission, martensitic transition



## Synchrotron Mössbauer spectroscopy on Fe<sub>3</sub>S, FeO and natural almandine

KAMADA, Seiji<sup>1\*</sup>; HIRAO, Naohisa<sup>2</sup>; HAMADA, Maki<sup>3</sup>; SUZUKI, Nanami<sup>1</sup>; OHTANI, Eiji<sup>1</sup>; OHISHI, Yasuo<sup>2</sup>; MASUDA, Ryo<sup>4</sup>; MITSUI, Takaya<sup>5</sup>

<sup>1</sup>Tohoku Univ., <sup>2</sup>JASRI, <sup>3</sup>School of Nature system, College of Science and Engineering, Kanazawa University, <sup>4</sup>Research Reactor Institute, Kyoto Univ., <sup>5</sup>JAEA

The Earth's core is considered to be composed of an iron alloy with light elements since its density is smaller than that of pure iron under core conditions (e.g., Birch, 1964; Dubrovinsky et al., 2000). Although there are many candidates for these elements, such as H, C, O, Si, and S, sulfur in particular has been considered as one of the most plausible candidates. This is because it is depleted in the mantle, suggesting that it exists in the Earth's core (Murthy and Hall, 1970), and iron sulfides are found universally in iron meteorites, i.e., analogues of the Earth's core. Although the content of sulfur in the Earth's core is not known precisely, the sulfur content in the core is estimated to be at least a few wt% based on cosmic element abundances (McDonough, 2003) and high pressure partitioning experiments (e.g., Hillgren et al., 2000).

Since sulfur is one of the most plausible light elements, a compressibility and phase diagram in the Fe-FeS system has been studied (e.g., Campbell et al., 2007; Chen et al., 2007; Fei et al., 2000; Kamada et al., 2010; Li et al., 2001; Seagle et al., 2006). According to previous studies, Fe<sub>3</sub>S is stable from 21 GPa and at least up to 200 GPa. Therefore, Fe<sub>3</sub>S can be one of a candidate of the inner core materials. In addition, a synchrotron Mössbauer spectroscopy (SMS) and X-ray emission spectroscopic studies on Fe<sub>3</sub>S revealed a spin transition and magnetic transition between 20 and 25 GPa (Lin et al., 2004; Shen et al., 2003). It also showed an abnormal evolution of a and c axes with increasing pressure (Chen et al., 2007).

Synchrotron Mössbauer spectroscopy is a good probe of a small sample under high pressure to investigate magnetic properties and electronic states of Fe of core and mantle minerals. An energy domain Mössbauer spectroscopic system has been recently developed at the BL10XU, SPring-8. We have measured Mössbauer spectra from Fe<sub>3</sub>S and FeO under high pressure and a natural almandine at ambient pressure.

A powder mixture was made from <sup>57</sup>Fe (96.63%, ISOFLEX) and FeS (99.9%, RAREMETALLIC co., LTD.) with a ratio of Fe:S=75.0:25.0 (in at%). A foil was made from the mixture by a cold compression using a diamond anvil cell (DAC) and loaded into a sample chamber. <sup>57</sup>Fe enriched Fe<sub>3</sub>S was synthesized from the powder mixture in a DAC at 30 GPa and 1350 K. The synthesis of Fe<sub>3</sub>S was confirmed by X-ray diffraction patterns at BL10XU, SPring-8. <sup>57</sup>FeO was made by reducing from <sup>57</sup>Fe<sub>2</sub>O<sub>3</sub> (ISOFLEX) at ambient pressure and high temperature. A pellet was made from <sup>57</sup>FeO powder and loaded into a sample chamber of a DAC. We also measured Mössbauer spectra of a natural almandine (Py<sub>15.7</sub>Alm<sub>78.6</sub>Gros<sub>4.4</sub>Sp<sub>1.3</sub>, Idaho, USA). The energy of used X-ray for Mössbauer spectroscopy was 14.4125 keV.

We have measured Mössbauer spectra of Fe<sub>3</sub>S during decompression at 5, 15, 20, 25, and 30 GPa and room temperature at BL10XU and BL11XU. At BL10XU, those of FeO and the almandine were obtained at 200 GPa and ambient pressure, respectively. The magnetic transition in Fe<sub>3</sub>S was observed between 20 and 25 GPa, which is consistent with Lin et al. (2004). We observed doublet peaks from FeO. An evidence of Fe<sup>3+</sup> in the almandine was not detected in this study. We will report the results of the Mössbauer spectra based on the newly developed system at BL10XU, SPring-8.

Keywords: Earth's core, Mantle, Mössbauer, Fe<sub>3</sub>S, FeO

## Temperature dependence of Fe<sup>3+</sup>, Al and Ga distributions and local domain structure in synthetic Ca-clinopyroxene

AKASAKA, Masahide<sup>1\*</sup>; HAMADA, Maki<sup>2</sup>; NAGASHIMA, Mariko<sup>3</sup>; EJIMA, Terumi<sup>4</sup>

<sup>1</sup>Dep. Geoscience, Shimane Univ., <sup>2</sup>School of Nature system, Kanazawa Univ., <sup>3</sup>Dept. Earth Sci., Yamaguchi Univ., <sup>4</sup>AIST

Distribution of Fe<sup>3+</sup>, Al<sup>3+</sup> and Ga<sup>3+</sup> among octahedral and tetrahedral sites in synthetic esseneite (CaFeAlSiO<sub>6</sub>)- and (CaFe<sup>3+</sup>GaSiO<sub>6</sub>)<sub>90</sub>(CaGa<sub>2</sub>SiO<sub>6</sub>)<sub>10</sub>-clinopyroxenes at 800 and 1200 °C were investigated using <sup>57</sup>Fe Mössbauer and X-ray Rietveld methods to find a relation between site occupancies of trivalent cations at the octahedral and tetrahedral sites and ionic sizes of trivalent cations. The esseneite was synthesized from oxide mixture using sintering technique at 1200 °C in air. The FeGaTs<sub>90</sub>GaTs<sub>10</sub>-Cpx was crystallized from glass starting material at 1200 °C in air. The Cpxs synthesized and those annealed at 800 °C were analyzed using <sup>57</sup>Fe Mössbauer spectroscopic and X-ray Rietveld methods. In the synthetic esseneite, <sup>V</sup>Fe<sup>3+</sup>:<sup>IV</sup>Fe<sup>3+</sup>-ratio at 800 °C was determined as 82(1):18(1) by Mössbauer method and 78.2(5):21.8(5) by Rietveld method, whereas, at 1200 °C, 79(1):21(1) by Mössbauer method and 77(1):23(1) by Rietveld analysis. The resulting Fe<sup>3+</sup> populations at octahedral M1 and tetrahedral T sites in the synthetic esseneite are Fe<sup>3+</sup>0.782(5)-0.82(1) apfu and 0.218(5)-0.18(1) apfu, respectively. In the synthetic Fe<sup>3+</sup>-Ga-Cpx, <sup>V</sup>Fe<sup>3+</sup>:<sup>IV</sup>Fe<sup>3+</sup>-ratio at 800 °C was 74(3):26(2) (Mössbauer analysis data) and 78(1):22(1) (Rietveld analysis data), while, at 1200 °C, 71(3):29(1) (Mössbauer analysis data) and 67(1):33(1) (Rietveld analysis), which results in populations at the octahedral M1 and tetrahedral T sites of [Fe<sup>3+</sup><sub>0.67(1)-0.70(1)</sub>Ga<sub>0.33-0.30</sub>]<sup>M1</sup>[Si<sub>1.0</sub>Fe<sup>3+</sup><sub>0.23-0.20</sub>

Ga<sub>0.77-0.80</sub>]<sup>T</sup> (O = 6) at 800 °C, and [Fe<sup>3+</sup><sub>0.64(1)-0.60(1)</sub>Ga<sub>0.36-0.40</sub>]<sup>M1</sup>[Si<sub>1.0</sub>Fe<sup>3+</sup><sub>0.26-0.30</sub>Ga<sub>0.74-0.70</sub>]<sup>T</sup> at 1200 °C. This result indicates the temperature dependence of Fe<sup>3+</sup>, Al<sup>3+</sup> and Ga<sup>3+</sup> distributions between M1 and T sites. However, it is evident that, even at different temperatures, distributions of Fe<sup>3+</sup>, Al<sup>3+</sup> and Ga<sup>3+</sup> between M1 and T sites are well correlated with the ratio of ionic radius of larger Fe<sup>3+</sup>-cation against smaller Al<sup>3+</sup> and Ga<sup>3+</sup>, as Akasaka et al. (1997) indicated. Another finding in this study is the splitting of a <sup>57</sup>Fe Mössbauer doublet by Fe<sup>3+</sup> at M1 site into two doublets. This indicates existence of short-range domain structure by two kinds of M1 sites with slightly different distortions, which cannot be detected by X-ray diffraction.

Keywords: clinopyroxene, Mossbauer analysis, X-ray structural refinement, Crystal chemistry, ionic distributions, temperature dependence

## Phase Transformation of Zirconium under High P-T Conditions

ONO, Shigeaki<sup>1\*</sup>

<sup>1</sup>JAMSTEC

The behavior of zirconium metal under high pressures is important in the community of the high-pressure study, because changes in resistivity due to the phase transformations of zirconium (Zr) are used as pressure calibration points in the high-pressure experiments. Zirconium metal, which shows the hcp structure at ambient conditions, is known to transform to the bcc structure (beta phase) above 1135 K at ambient pressure. With increasing pressure, phase transformations to a hexagonal structure (omega phase), at the pressure around 5 GPa and to a bcc structure around 30 GPa have been observed at room temperature. The formation of the high-pressure phases is concerned with changes in the electronic structure. Recent investigations for the phase transformation from the hexagonal to the bcc structures at high temperatures (Zhang et al. 2005 and 2007) were inconsistent with previous study at temperatures around the room-T (Xia et al. 1991). Therefore, we reinvestigated the transformation pressure in zirconium metal.

The starting material used in this study was polycrystalline Zr. High-pressure X-ray diffraction experiments were carried out in an external heated diamond anvil cell. The small sample sandwiched between pellets of NaCl powder was loaded into a hole that had predrilled into a rhenium gasket. The heating temperature was up to 800 K, and was recorded using the R-type of thermocouples. The sample was probed using angle-dispersive X-ray diffraction, located on the synchrotron beam lines, at NE1A of the Photon Factory. Details of the synchrotron X-ray experiments have been described elsewhere (e.g., Ono et al. 2005). The angle-dispersive X-ray diffraction patterns were obtained on the imaging plate of an X-ray data collection system (Rigaku, RAXIS). The pressure was calculated from the NaCl unit cell volume using the equation of state (EOS) for NaCl, as developed by Ono (2010).

The boundary from the omega phase to the bcc phase was determined at high temperatures (300 - 800 K). Our results were in good agreement with those reported in previous room-temperature study. The gradient of  $dP/dT$  of the boundary was negative. However, the gradient observed in our experiments was 2-3 times more negative than that reported by previous high-temperature experiments (Zhang et al. 2005 and 2007). Our new data indicated that the difference in the stress conditions of the sample led to the discrepancy of the gradient of  $dP/dT$  slope in previous studies.

Keywords: Zirconium, Phase transition, High pressure and high temperature

## Crystal structure analysis of a new high-pressure strontium silicate

SEKINE, Keisuke<sup>1</sup> ; ISHII, Takayuki<sup>1</sup> ; KOJITANI, Hiroshi<sup>1\*</sup> ; AKAOGI, Masaki<sup>1</sup>

<sup>1</sup>Dept. of Chemistry, Gakushuin University

SrSiO<sub>3</sub> is an analog material to CaSiO<sub>3</sub> which is an important component of the Earth's crust- and mantle-constituting minerals. High-pressure phase relation experiments in SrSiO<sub>3</sub> showed that δ'-SrSiO<sub>3</sub> is stable up to about 10 GPa and decomposes into BaGe<sub>2</sub>O<sub>5</sub>-III -type SrSi<sub>2</sub>O<sub>5</sub> + larnite-type Sr<sub>2</sub>SiO<sub>4</sub> between 14 and 20 GPa (Kojitani et al., 2005). Then, hexagonal perovskite-type SrSiO<sub>3</sub> becomes stable above about 20 GPa (Yusa et al., 2005). However, phases except for larnite-type Sr<sub>2</sub>SiO<sub>4</sub> appearing in the pressure range between 10 and 14 GPa have been unclear. In this study, crystal structure and composition of one of the unknown phases were determined.

A sample for single-crystal structure analysis was synthesized by heating a mixture of pseudowollastonite-type CaSiO<sub>3</sub> and SiO<sub>2</sub> cristobalite (mole ratio of 1:1) with a little amount of water at 12 GPa and 1200 °C for 90 min using a Kawai-type multi-anvil high-pressure apparatus. A single-crystal sample with 120x80x60 μm was used for the single-crystal X-ray diffraction measurement. 953 reflection data were analyzed using the SHELX-97 software. Composition analysis of the high-pressure phase was performed using SEM-EDS.

The composition analysis showed that the new high-pressure phase had a composition of Sr<sub>4</sub>Si<sub>9</sub>O<sub>22</sub>. The single-crystal structure analysis suggests the monoclinic crystal system with the space group of *C2/m*. Lattice parameters were determined to be  $a = 13.3765(4) \text{ \AA}$ ,  $b = 5.2321(2) \text{ \AA}$ ,  $c = 11.6193(6) \text{ \AA}$ ,  $\beta = 113.976(4) \text{ deg}$ . *R* factor was 1.25%. The framework of the obtained crystal structure consists of two layers by corner-sharing single chains of edge-shared SiO<sub>6</sub> octahedra or SiO<sub>5</sub> rhombic pyramid polyhedra and by corner-shared SiO<sub>4</sub> tetrahedra and SiO<sub>6</sub> octahedra. It should be mentioned that this structure includes the SiO<sub>5</sub> rhombic pyramids which are very rare in silicates. Strontium ions in the structure are arranged between the two layers and are coordinated by seven oxygens. The structure of δ'-SrSiO<sub>3</sub> consists of four-membered rings of SiO<sub>4</sub> tetrahedra and strontium ions coordinated by seven oxygens. On the other hand, BaGe<sub>2</sub>O<sub>5</sub>-III type SrSi<sub>2</sub>O<sub>5</sub> has a framework by corner-shared SiO<sub>6</sub> octahedra and SiO<sub>4</sub> octahedra and coordination number of Si<sup>2+</sup> is 12. The crystal structure determined in this study is consistent with the fact that its density would be between those of the lower-pressure and higher-pressure phases.

Keywords: strontium silicate, high-pressure, single-crystal structure analysis, SiO<sub>5</sub> polyhedron

## Heat capacity and entropy measurements by PPMS for high-pressure phases in TiO<sub>2</sub> and MnSiO<sub>3</sub>

AKAOGI, Masaki<sup>1\*</sup> ; KOJIMA, Meiko<sup>1</sup> ; FUKAI, Aya<sup>1</sup> ; KOJITANI, Hiroshi<sup>1</sup>

<sup>1</sup>Dept. of Chemistry, Gakushuin University

Thermodynamic properties of high-pressure minerals are widely used to calculate phase relations at high pressures and high temperatures and to compare with the properties by the first-principles calculations. Standard entropy,  $S_{298.15}$ , is determined by integrating  $C_p/T$  in the temperature range between 0 and 298.15 K, where  $C_p$  is isobaric heat capacity and  $T$  is absolute temperature. To measure  $C_p$  at the temperature range, adiabatic calorimetry has been widely used with the highest precision. However,  $C_p$  of only a few high-pressure minerals have been measured so far, because a sample of more than several gram is required for the adiabatic calorimetry. Recently, low-temperature  $C_p$  measurement with thermal relaxation method using the Physical Properties Measurement System (PPMS) has been developed for samples of about ten milligram quantity. In this method, the sample is cooled with liquid helium and  $C_p$  is measured at about 2-310 K. By measuring the sample temperature change associated with applied heat pulse, thermal relaxation process is analyzed to obtain  $C_p$ . By this method, we measured  $C_p$  and determined  $S_{298.15}$  for Mg<sub>2</sub>SiO<sub>4</sub> wadsleyite and ringwoodite, MgSiO<sub>3</sub> akimotoite and perovskite, and SiO<sub>2</sub> stishovite, in collaboration with Atake-Kawaji laboratory, Tokyo Institute of Technology. Very recently, we have installed the PPMS apparatus in the laboratory in Gakushuin University, and have investigated  $C_p$  and  $S$  of rutile-type and  $\alpha$ -PbO<sub>2</sub>-type TiO<sub>2</sub> and garnet-type MnSiO<sub>3</sub>.

Using a multianvil apparatus, rutile- and  $\alpha$ -PbO<sub>2</sub>-type TiO<sub>2</sub> phases were synthesized at 3 and 8 GPa, respectively, at 600-700 °C, and MnSiO<sub>3</sub> garnet was made at 15 GPa and 1000 °C. All the cylindrical samples were polished and fixed with grease on the stage in the PPMS. The  $C_p$  measurements in this study were performed at 2-308 K using the polycrystalline samples of 10-21 mg. The  $C_p$  measured for  $\alpha$ -Al<sub>2</sub>O<sub>3</sub> (NBS SRM-720) by the PPMS apparatus were consistent within experimental errors with those measured by adiabatic calorimetry by Ditmars et al. (1982).

The measured  $C_p$  of rutile-type TiO<sub>2</sub> were in good agreement with those by previous studies, and the obtained  $S_{298.15}$  was 50.10 J/molK. Our  $C_p$  data of  $\alpha$ -PbO<sub>2</sub>-type TiO<sub>2</sub> were almost consistent with those with PPMS measurement by Yong et al. (2014), but substantially smaller than those with DSC measurement by Manon (2008). The  $S_{298.15}$  of  $\alpha$ -PbO<sub>2</sub>-type TiO<sub>2</sub> was determined as 46.50 J/molK in this study. The  $C_p$  data of MnSiO<sub>3</sub> garnet indicated an anomaly at 15 K probably due to magnetic transition, and  $S_{298.15}$  of 90.92 J/molK. High-pressure phase relations calculated using the above data are also reported.

Keywords: heat capacity, entropy, high-pressure phase, PPMS apparatus

## Mechanisms of phase transitions of methane hydrate under high pressure

KADOBAYASHI, Hirokazu<sup>1\*</sup>; HIRAI, Hisako<sup>1</sup>; HIRAO, Naohisa<sup>2</sup>; OHISHI, Yasuo<sup>2</sup>; OHTAKE, Michika<sup>3</sup>; YAMAMOTO, Yoshitaka<sup>3</sup>; KOJIMA, Yohei<sup>1</sup>

<sup>1</sup>Geodynamics Research Center, Ehime University, <sup>2</sup>Japan Association of Synchrotron Radiation Institute, <sup>3</sup>National Institute of Advanced Industrial Science and Technology

Methane hydrate (MH), called as “ burning ice ”, is expected to be a fruitful natural resource, at the same time, methane is rather effective greenhouse gas than carbon dioxide. It is also thought to be a major constituent of icy bodies in and outside the solar system. MH is composed of hydrogen-bonded host water molecules forming cages or frameworks that include guest methane molecules. Three phases of MH have been known so far. The low-pressure phase, sI, is stable below 0.8 GPa and it transforms into a hexagonal structure, sH, at 0.8 GPa and further transforms to a filled ice Ih (FIIhS) at 1.8 GPa at room temperature. At these phase transitions, release of water content is accompanied. As described above, the existence of phase transitions and the structures of transformed high-pressure phases have been clarified by the previous studies. However, transition mechanisms from the lower-pressure phase to individual high-pressure phases have been unresolved issue. In this study, high-pressure experiments were performed to investigate mechanisms of the phase transitions of MH at high pressures.

Clamp type and lever-spring type diamond anvil cells were used in this study. The pressure and temperature conditions were from 0.2 to 3.0 GPa and 300 K, respectively. Pressure measurements were made via a ruby fluorescence method. The initial samples of MH were prepared by ice-gas interface method. The samples were characterized via time-resolved X-ray diffractometry using synchrotron radiation at BL-10XU, SPring-8, and time-resolved Raman spectroscopy at GRC, Ehime University.

As for sI-sH phase transition, Raman spectroscopy revealed that  $5^{12}$  cages of sI survived during the transition and that the  $5^{12}$  cages remained as same  $5^{12}$  cages of sH structure. And,  $5^{12}6^2$  cages of sI changed to  $4^35^66^3$  and  $5^{12}6^8$  cages of sH. The results suggested that the sI-sH transition may follow a martensitic-like mechanism because of being maintaining  $5^{12}$  cages unchanged in sH structure. On the other hand, at sH-FIIhS transitions, Raman spectroscopy detected abrupt collapse of all constituent cages in sH and release of fluid or solid methane molecules. And then, the framework of FIIhS was gradually reconstructed, absorbing the released methane molecules into the FIIhS structure. The results indicated that the sH-FIIhS transition follows reconstructive mechanism. The explanations may be reasonable, because the former transition is from a cage to another cage structure, and the latter one is from a cage structure to different framework of a filled ice structure.

Keywords: methane hydrate, mechanisms of phase transitions, high-pressure, X-ray diffractometry, Raman spectroscopy

## Incorporation of NaCl into ice VI and ice VII under high pressure.

HIRAI, Hisako<sup>1\*</sup> ; YAMASHITA, Fukunori<sup>1</sup> ; KAGAWA, Shingo<sup>1</sup> ; KADOBAYASHI, Hirokazu<sup>1</sup> ; OHISHI, Yasuo<sup>2</sup> ; YAMAMOTO, Yoshitaka<sup>3</sup>

<sup>1</sup>Geodynamics Research Center, Ehime University, <sup>2</sup>JASRI, <sup>3</sup>AIST

Icy satellites have been thought to contain a large amount of salts besides water ices. Ice exhibits a wide variety of forms consisting of hydrogen-bonded water molecules. More than sixteen stable and metastable forms have been reported so far. Liquid water can dissolve various kinds of solutes. Whereas, in the previous idea, when water crystallizes, the dissolved solutes are excluded, which results in formation of pure water ices. Recently, Frank et al. [1] and Komatsu et al. [2] reported that NaCl or other salts was incorporated into ice VI and/or ice VII. In these studies, however, it has been still unclear which ice can incorporate NaCl, and amount of salts incorporated and states of the salt in the ice structure have not yet been clarified. In this study, in order to understand possible incorporation of salts in to ice VI and VII structures, high-pressure experiments were performed with a system of H<sub>2</sub>O-NaCl, a typical salt, at room temperature.

Lever-and-spring type diamond anvil cell was used. Pressure range examined was from 0.2 to 10 GPa. NaCl aqueous solutions with three concentrations, 1.5, 2.5, and 5.0 w%, were prepared as starting samples. Characterization was made by optical microscopy, X-ray diffractometry (XRD), and Raman spectroscopy.

Similar phase changes were observed for the samples with three different concentrations. The NaCl aqueous solutions finally crystallized to form ice VI above 1.6 GPa, although in case of pure water ice VI is formed at 1.0 GPa at room temperature. At the pressure range from 2.1 to 3.2 GPa, a new high-pressure phase, of which diffraction pattern was not explained by ice VI, ice VII, and solid NaCl, was observed. Above 3.2 GPa, ice VII and solid NaCl appeared. The high-pressure phase observed may correspond to a phase having a modified structure of NaCl-dihydrate reported by Nakayama et al. [3]. Unit cell volumes of ice VII calculated expanded larger than those of pure ice VII. The result was opposite sense to those by Frank et al, where the volumes decreased smaller than those of pure ice VII. The amounts of the volume expansion for 2.5 and 5.0 w% samples were larger than those of 1.5 w% samples. The volume expansions of the former two samples were almost similar. The results suggested that limitation of incorporation into ice VII is less than 2.5 w%. The O-H vibrational modes shifted to higher frequencies by 10 to 20 cm<sup>-1</sup> and 5 to 10 cm<sup>-1</sup> from those of pure ices for ice VI and ice VII, respectively.

All experimental results indicated that NaCl is incorporated both into ice VI and ice VII at room temperature. The amounts of incorporation were estimated to be up to 2.5 w%. Such large amount of incorporation of salt is expected to effect on physical properties of ices, which is important in inferring the interiors of icy bodies.

1. M. R. Frank et al., PEPI 155 (2006) 152; M. R. Frank et al., PEPI 170 (2008) 107; M. R. Frank et al., PEPI 215 (2013) 12.
2. K. Komatsu et al., Abstract of Annual meeting of Jpn. Society High Pressure Tech. (2010).
3. K. Nakayama master thesis (2012).

Keywords: high-pressure ice, NaCl, incorporation, icy satellite

## Structure refinement of legrandite and paradamite : crystal chemistry and hydrogen bonds

JINNOUCHI, Satoshi<sup>1\*</sup> ; YOSHIASA, Akira<sup>1</sup> ; SUGIYAMA, Kazumasa<sup>2</sup> ; ARIMA, Hiroshi<sup>2</sup> ; SHIMURA, Reiko<sup>2</sup> ; MIYAWAKI, Riturou<sup>3</sup>

<sup>1</sup>Graduate School of Science and Technology, Kumamoto University., <sup>2</sup>Institute for Materials Research, Tohoku University,  
<sup>3</sup>National Science Museum

Legrandite,  $Zn_2AsO_4(OH)H_2O$  and paradamite,  $Zn_2AsO_4(OH)$ , are zinc arsenate minerals and have a color between pale yellow and yellowish brown. Related minerals of legrandite and paradamite are adamite,  $Zn_2AsO_4(OH)$ , and so on with different structures. We performed the structure refinement of legrandite and paradamite Oujela Mine, Mapimi, Durango, Mexico, by (RAPID) RIGAKU single-crystal structure analysis system. We determined the hydrogen position by difference Fourier method. We revealed the detail hydrogen bond using bond valence calculation and hydrogen positions and compared crystal structures of these. The structure of legrandite is constituted by two  $AsO_4$  tetrahedrons,  $ZnO_6$  octahedron and three  $ZnO_5$  trigonal dipyramids that have large unique distortion.  $AsO_4$  tetrahedron,  $ZnO_5$  trigonal dipyramid and  $ZnO_6$  octahedron constitutes the unique framework. The structure of paradamite is constituted by  $AsO_4$  tetrahedron and two  $ZnO_5$  trigonal dipyramid that have large unique distortion. In legrandite, 5 coordination of trigonal dipyramids have a distance to be expected from ionic radii but interatomic distance of Zn(3)-O(1) has extraordinary distance. Two OH groups bond to Zn1 and Zn2, Zn3 and Zn4 make the  $ZnO_3(H_2O)_2$  trigonal dipyramid that is bonded to two  $H_2O$  group in legrandite. In paradamite, Zn1 and Zn2 make  $ZnO_3(OH)_2$  and  $ZnO_4(OH)$  trigonal dipyramid. Hydrogen atoms make a lot of hydrogen bonding in legrandite and paradamite. Crystal structure of legrandite has a tunnel structure continuous that is only parallel to c axis and similar structure is observed in paradamite only parallel to a axis. There are path of proton-conduction in these direction and we conjecture that these proton-conductivity have large anisotropy of one dimension.

Keywords: structure refinement, legrandite, paradamite, crystal chemistry, hydrogen bonds

## Structure analysis of deuterated brucite at pressures to 3 GPa by pulsed neutron powder diffraction

OKUCHI, Takuo<sup>1\*</sup> ; TOMIOKA, Naotaka<sup>1</sup> ; PUREVJAV, Narangoo<sup>1</sup> ; HARJO, Stefanus<sup>2</sup> ; ABE, Jun<sup>3</sup> ; WU, Gong<sup>2</sup>

<sup>1</sup>Institute for Study of the Earth's Interior, Okayama University, <sup>2</sup>Japan Atomic Energy Agency, <sup>3</sup>CROSS Tokai

Atomic-scale structures around hydrogen atoms in hydrous minerals may significantly change with increasing pressure, which affect thermodynamic stability, optical properties (Raman, IR, etc.), and transport phenomena of the relevant minerals. To directly observe such structure change around hydrogen atoms, we have conducted neutron diffraction experiments of deuterated brucite at high pressures to 2.8 GPa, using a high-resolution neutron powder diffractometer recently installed at J-PARC Materials and Life Science Experimental Facility. To discriminate subtle structure change of deuterium site positions with increasing pressure, the quality of observed diffraction patterns has been considerably improved from the corresponding previous studies by adopting a new-type experimental apparatus and facility. A newly-designed opposed anvil cell apparatus optimized for the pulsed neutron beam (Okuchi et al., *High Pressure Research*, 33, 777, 2013) was effectively coupled with the time of flight diffractometer TAKUMI, which was designed to have the resolution of  $\Delta d / d \sim 0.3\%$  along with moderately-intense beam and low background (Harjo et al., *Materials Science Forum*, 524, 199). We used single crystal diamond anvils with culet diameter of 2 mm for sample compression along with deuterated glycerine pressure medium. The combination gives very high neutron transparency as well as high resolution to enable accurate structure refinements of tiny sample volume of the order of less than 1 mm<sup>3</sup>. Through Rietveld refinements of the observed patterns, tilting of all OD dipoles in the compressed brucite toward one the three nearest-neighbor oxygen anions in the brucite structure was confirmed to be substantial at the observed pressure regime, suggesting the formation of pressure-induced hydrogen bonding. Therefore, at lower crust and mantle wedge conditions, this pressure-induced bonding may play an important role to constrain hydrogen into the relevant hydrous minerals.

Keywords: hydrogen, brucite, high pressure, neutron diffraction

## Factors controlling barite-water distribution of selenium oxyanion

TOKUNAGA, Kouhei<sup>1\*</sup>; YOKOYAMA, Yuka<sup>1</sup>; TAKAHASHI, Yoshio<sup>1</sup>

<sup>1</sup>Department of Earth and Planetary Systems Science, Graduated School of Science, Hiroshima University

Geochemical behavior of trace elements is controlled by their interaction with major minerals through ion exchange, sorption/desorption, and coprecipitation/dissolution processes, which govern the concentrations of trace elements in natural water. Especially, the coprecipitation process with mineral is potentially important because trace elements can be incorporated and immobilized in the crystal lattice at least until the minerals are dissolved. Previous studies showed that the partitioning behaviors of trace elements to minerals were controlled by many complex factors, such as crystal constraints of ion substitution, effects of complexation in the aqueous phase, rate of crystallization, and changes in temperature or pressure. For instance, Yokoyama [2011, 2012] demonstrated that, in the case of arsenic (As) and selenium (Se) incorporation into calcite, arsenate rather than arsenite is selectively incorporated into calcite, whereas selenite (Se(IV)) rather than selenate (Se(VI)) into calcite because of the high stabilities of calcium arsenate and calcium selenate complexes compared with those for arsenite and selenite. In this study, we focused on the distribution behavior of Se into barite to determine the factors controlling the partitioning behaviors of the trace elements to minerals at the molecular scale by X-ray absorption fine structure (XAFS). Our previous results suggested that the distribution behavior of Se into barite was controlled by two factors: the stability of the surface complex between barite and Se species (=chemical affinity) at the initial process and the stability of the ion substitution in the crystal structure (=structural affinity) for the subsequent process. In this presentation, the barite-water distributions of Se controlled by the structural affinity are highlighted.

The coprecipitation experiments were conducted to examine the influence of ion substitution structure on the distribution behavior of Se into barite as a function of the reaction time in term of the variation of barite morphology, total concentration, oxidation states, and coordination structure of Se in barite. The results showed that both total Se concentration and the Se(VI)/Se(IV) ratio in barite increased abruptly within first 24 hour and almost reached equilibrium after 24 hours. EXAFS analysis for the initial and aged samples showed that the coordination number of Se-Ba in the aged sample is larger than that in the initial stage. The results indicates that a larger amount of Se(VI) than Se(IV) was incorporated from adsorption site on the surface into the barite crystal by substituting sulfate site because of their high crystallinity that can excludes Se(IV) to a larger degree than Se(VI) due to the similar structure of sulfate ion and sulfate. Based on these results, it is considered that the Se(VI) was preferentially incorporated into barite due to its high structural affinity than Se(IV), thus, the Se(VI)/Se(IV) ratios in barite relatively increased through crystallization. These results suggest that structural affinity is an important factor for controlling the distribution behavior of Se between barite and water.

Keywords: barite, selenite, selenate, XAFS, distribution behavior, structural affinity

## Mid- and far-infrared spectroscopy for Li-Al-Mg micas

MAKIO, Masato<sup>1\*</sup> ; ISHIDA, Kiyotaka<sup>1</sup>

<sup>1</sup>Graduate School of Social and Cultural Studies

Mica is a one of the major rock forming minerals and widely spread in the earth crust. The hydrothermal synthetic Li-Al-Mg trioctahedral mica series were measured by mid- and far-infrared spectroscopy and X-ray powder diffraction Rietveld refinement: (a)Trilithionite:  $K(Li_{1.5}Al_{1.5})(AlSi_3)O_{10}F_2$ - Phlogopite:  $KMg_3(AlSi_3)O_{10}F_2$ , (b)Polyolithionite:  $K(Li_2Al)Si_4O_{10}F_2$ - Tainiolite:  $K(LiMg_2)Si_4O_{10}F_2$ , (c)Polyolithionite- Eastonite:  $K(Mg_2Al)(Al_2Si_2)O_{10}F_2$  and OD- FMg- Masutomilite:  $K(LiAlMg)AlSi_3O_{10}(F, OD)_2$ .

The Li-Al-Mg micas synthesized hydrothermally at 600- 650 °C and 150- 200MPa in cold-seal externally heated Tuttle-type vessels. The starting materials were mixed and then sealed in Pt/Au capsules with 20 wt % D<sub>2</sub>O (99.9 % in purity). X-ray Rietveld analysis was done using Rietan- 2000 (Izumi and Ikeda 2000). Mid- and far-infrared spectra were measured with JASCO FTIR- 620 spectrometer. Each sample was scanned 256 times in an evacuated sample-chamber.

All samples could refine monoclinic, C2/m (1M polytype). In the 250- 50cm<sup>-1</sup> far-infrared region, three kinds of bands are observed: these bands due to an in- plane tetrahedral torsional band between 170- 150cm<sup>-1</sup>, an interlayer K- O<sub>inner</sub> stretching band between 120- 140 cm<sup>-1</sup> and K- O<sub>outer</sub> stretching band between 90- 100 cm<sup>-1</sup>. With increasing <K- O<sub>inner</sub>>, K- O<sub>inner</sub> stretching band shifts higher frequency, while with increasing <K- O<sub>outer</sub>>, K- O<sub>outer</sub> stretching band shifts lower frequency. In the 650- 250cm<sup>-1</sup> mid- and far-infrared region, two parts of bands are observed. With increasing <sup>[4]</sup>Si→Al, (Si,Al)- O deformational band in the range of 600- 400cm<sup>-1</sup> became broad and merged.

Keywords: Li-Al-Mg mica, hydrothermal synthesis, mid-infrared, far-infrared, Rietveld analysis

## Cesium (Cs) Sorption Experiments into Weathered Biotite in Fukushima

KIKUCHI, Ryosuke<sup>1\*</sup> ; KOGURE, Toshihiro<sup>1</sup>

<sup>1</sup>Earth and Planetary Sci., Univ. Tokyo

After the accident of Fukushima Daiichi nuclear power plant in March 2011, radioactive contamination of the soil around the plant has become an urgent problem in Japan. Previous studies proposed that weathered micaceous minerals present favorable sorption environments for Cs<sup>+</sup>. Because the contaminated areas in Fukushima are mainly covered with weathered granite soil, weathered biotite with hydrated (vermiculite) interlayers is abundant. Hence basic understanding of Cs<sup>+</sup> sorption process into the biotite is important to find the recipe for decontamination of radiation. Some of previous studies reported that Cs<sup>+</sup> is adsorbed mainly at the frayed-edge sites of such micaceous crystals. However, other studies indicated that Cs<sup>+</sup> penetrates deeply inside the crystals, along the interlayer regions by ion-exchange. In this study, we performed Cs<sup>+</sup> sorption experiments using single-crystals of Fukushima weathered biotite with well-regulated edge surfaces, and considered the relationship between the weathering state of biotite and Cs<sup>+</sup> sorption property.

Fresh and two kinds of weathered biotite were collected from granodiolite of Abukuma granite body in Fukushima prefecture. For each sample, cross sections of <1 mm thick perpendicular to the basal planes were prepared. Surface damage formed by the mechanical grinding/polishing was removed by Ar<sup>+</sup> ion sputtering. These sections were immersed in 30 mL of CsCl aqueous solution of 2000 / 200 / 20 / 0 ppm for 24 hours at room temperature to incorporate Cs<sup>+</sup>.

After the reaction, the surfaces of the sections were investigated using scanning electron microscopy (SEM) with energy dispersive X-ray spectroscopy (EDS). SEM-EDS with various acceleration voltage indicated that the concentration of the sorbed Cs<sup>+</sup> does not change in the depth direction of ~several microns range. Cs<sup>+</sup> was apparently sorbed at 2000 ppm but not at 200 ppm for fresh biotite, whereas Cs<sup>+</sup> was sorbed at both concentrations in the weathered biotite. Back-scattered electron (BSE) images and EDS analysis showed preferred sorption of Cs<sup>+</sup> at the regions probably with dense vermiculite interlayers in the weathered biotite. Moreover, some specimens were processed into thin foils using focused ion beam (FIB) and examined using scanning transmission electron microscopy (STEM). High-angle annular dark field (HAADF) imaging in STEM has visualized Cs<sup>+</sup>-incorporated interlayer regions individually in the weathered biotite.

Keywords: Biotite, Vermiculite, Cesium, SEM-EDS, FIB, HAADF-STEM

## Pressure-induced phase transitions of vaterite, a metastable phase of calcium carbonate

MARUYAMA, Koji<sup>1\*</sup>; KOMATSU, Kazuki<sup>1</sup>; KAGI, Hiroyuki<sup>1</sup>; YOSHINO, Toru<sup>2</sup>; NAKANO, Satoshi<sup>3</sup>

<sup>1</sup>Geochemical Research Center, Univ. Tokyo, <sup>2</sup>TIRI, <sup>3</sup>National Institute for Materials Science

### 1. Introduction

Calcium carbonate is one of the most common and ubiquitous minerals on the Earth's surface and plays an important role in global carbon cycle. There are many studies about high-pressure behavior of calcite and aragonite. At ambient temperature, calcite transforms to calcite II at about 1.5 GPa and to calcite III at about 2.0 GPa. The transition from aragonite to post-aragonite phase was observed at about 40 GPa. In contrast, no study has been reported on the high-pressure behavior of vaterite, which is a metastable phase of CaCO<sub>3</sub>, and is known as a precursor material of more stable CaCO<sub>3</sub> polymorphs, calcite and aragonite. In this study, the high-pressure behavior of vaterite was investigated by in situ synchrotron X-ray diffraction (XRD) experiments using a diamond anvil cell.

### 2. Experimental method

In this study, vaterite was synthesized by mixing two aqueous solutions, 60 mM CaCl<sub>2</sub> aq. and 60 mM NaHCO<sub>3</sub> aq., kept at 30 degree C. The mixed solution was sealed in a plastic bottle and stirred for 10 min at 30 degree C, and then filtered using an aspirator, washed by pure water, and dried at about 130oC. The obtained white powder was identified as pure vaterite using powder XRD method.

High-pressure experiments were carried out using a diamond anvil cell (DAC). The synthesized vaterite and several tiny ruby crystals were loaded into a gasket hole together with helium as a pressure transmitting medium. The pressure was changed between 0-14 GPa, which was measured by the ruby fluorescence method. XRD patterns were measured at each pressure at room temperature. X-ray diffraction observations were carried out at room temperature using the synchrotron beam line of BL18C in the Photon Factory, Japan.

### 3. Results and discussion

XRD patterns recorded at pressures lower than 4.7 GPa indicated that the sample consists of vaterite only. At 4.7 GPa, main three peaks of vaterite were split and a peak assignable to calcite III appeared. The discontinuous changes in axial lengths were observed by refinement of lattice constants using a crystal structure model proposed by Le Bail et al. (2011). This change suggests a pressure-induced phase transition from vaterite to a high-pressure form (hereafter vaterite II). Change in the diffraction intensities suggested that vaterite II transformed to calcite III with increasing pressure up to about 9 GPa. At 12.9 GPa, new diffraction spots were observed. These spots were not explainable with the diffraction peaks from any polymorphs of CaCO<sub>3</sub>. This implies that the new spots are derived from another high-pressure phase of vaterite (vaterite III). After decompression, the recovered sample was identified as a mixture of calcite and vaterite. These results indicate that the transition from vaterite II to calcite III is irreversible. In this study, new high-pressure phases of CaCO<sub>3</sub> (vaterite II and III) were discovered by high-pressure experiments of vaterite at ambient temperature.

Keywords: vaterite, phase transition, high-pressure

## Huge plastic deformation of SiO<sub>2</sub> glass at room temperature

WAKABAYASHI, Daisuke<sup>1\*</sup> ; FUNAMORI, Nobumasa<sup>1</sup> ; SATO, Tomoko<sup>2</sup>

<sup>1</sup>Department of Earth and Planetary Science, University of Tokyo, <sup>2</sup>Department of Earth and Planetary Systems Science, Hiroshima University

Covalent solids are known to be hard but brittle. Moreover, glasses do not deform plastically by dislocation movement seen in crystals due to the lack of long-range order. However, SiO<sub>2</sub> glass, a highly covalent glass, has long been known to be densified up to about 20% by applying high pressure. This phenomenon is called permanent densification, which is some kind of phase transformation caused by the reconstruction of the network structure consisting of SiO<sub>4</sub> tetrahedra [e.g., Wakabayashi et al., 2011], and could be considered as plastic deformation in a broad sense. Recently, the differential strain of SiO<sub>2</sub> glass in its intermediate-range structure, corresponding to the first sharp diffraction peak, was measured under uniaxial compression by a radial X-ray diffraction method, in which X-rays irradiate the sample from a direction perpendicular to the compression axis (i.e., from a radial direction) [Sato et al., 2013]. In those measurements, very large differential strains were observed under pressure and surprisingly also after decompression. This residual strain may be attributable to the anisotropic reconstruction of the network structure (i.e., anisotropic permanent densification).

In this study, the change in size of bulk samples was measured for uniaxially-compressed SiO<sub>2</sub> glass to clarify whether SiO<sub>2</sub> glass undergoes plastic deformation in a narrow sense, i.e., without density change. X-ray diffraction measurements were also conducted in a wide Q-range with 50 keV monochromatic X-rays by irradiating the recovered sample from the radial direction to clarify whether a differential strain remains only in the intermediate-range network structure or also in the short-range SiO<sub>4</sub> tetrahedral structure. Pressures were generated by using a diamond-anvil cell. The starting material was in the form of a disk, and was adjusted to have an appropriate initial thickness to be compressed under uniaxial conditions, i.e., pinched directly by the two anvils, above a certain pressure. Three independent experiments were conducted with an argon pressure medium up to 20 GPa in run 1, 12 GPa in run 2, and 6 GPa in run 3. The change in size of sample was measured with an optical microscope. X-ray diffraction measurements were carried out at PF AR-NE1. All the experiments were conducted at room temperature.

In runs 1 and 2, the diameter of sample was found to increase significantly with pressure from 6-8 GPa, where uniaxial conditions were achieved, to the maximum pressure of each run without fracturing, and it became about 15% larger at 20 GPa than at 0 GPa. The macroscopic differential strain was about an order of magnitude larger than the microscopic differential strain reported in the previous study [Sato et al., 2013], suggesting that SiO<sub>2</sub> glass deformed plastically at room temperature. The X-ray diffraction measurements clarified that the recovered samples were in the fully densified state (about 20% densified). It was also revealed that a residual differential strain was observed only in the intermediate-range network structure and its magnitude was consistent with the previous study [Sato et al., 2013]. On the other hand, in run 3, the sample did not deform plastically by uniaxial compression from 2-3 GPa to 6 GPa. The X-ray diffraction pattern of the recovered sample was the same as that of the ordinary SiO<sub>2</sub> glass. Permanent densification is known to begin at about 9 GPa under hydrostatic conditions [e.g., Wakabayashi et al., 2011], and it is suggested that permanently densified SiO<sub>2</sub> glass easily undergoes plastic deformation even at room temperature.

D. Wakabayashi et al., *Phys. Rev. B* **84**, 144103 (2011).

T. Sato et al., *J. Appl. Phys.* **114**, 103509 (2013).

Keywords: SiO<sub>2</sub> glass, plastic deformation, permanent densification, network structure

## Shock compression of synthetic amino acid - silica gel complex modeling for comet nucleus

MURAI, Takuro<sup>1</sup> ; OKUNO, Masayuki<sup>2\*</sup> ; OKUDERA, Hiroki<sup>2</sup> ; ARASUNA, Akane<sup>1</sup> ; MASHIMO, Tsutomu<sup>3</sup> ; CHEN, Liliang<sup>3</sup> ; MIZUKAMI, Tomoyuki<sup>2</sup> ; ARAI, Shoji<sup>2</sup>

<sup>1</sup>Graduate School of Kanazawa University, <sup>2</sup>Kanazawa University, <sup>3</sup>Kumamoto University

Some amino acids were found in comet coma particle and Murchison meteorite [1,2]. These reports may suggest a possibility that basic materials of primitive life on the earth were formed in the space and delivered to the earth.

Greenberg et al. (1997)[3] reported the almost comets are made of organic compounds, silicates and ice. On the other hand, silica gel contains a non crystalline  $\text{SiO}_{4-n}(\text{OH})_n$  framework with water molecules. So, silica gel is a suitable model material for comet. In this study, in order to investigate the stability of amino acid (L-serine) in the comet nucleus during the impact to the earth, synthetic amino L-serine - silica gel complex materials were shock compressed and the structure change of the recovered samples were analyzed by X-ray diffraction measurements, IR and Raman spectroscopies. Shock compression experiments were performed at 8.2, 10.9, 19.7 and 26.9 GPa.

By Raman spectroscopic analyses, it was indicated that synthetic complex materials include two types of L-serine such as crystalline L-serine and hydrated L-serine. Obtained Raman spectra of shocked materials show the L-serine crystal was disappeared and hydrated L-serine molecules survived at 19.7 GPa of shock pressure. Therefore, the sample at 19.7 GPa includes only hydrated L-serine molecules. This may indicate that intermolecular hydrogen bonds of L-serine molecules may be broken by shock compression with water molecule.

The shock pressure of 19.7 GPa is consistent with the estimated impact pressure of about 19% comets to the earth reported by Blank et al. (1999) [4]. This fact may indicate that a possibility for the basic materials of primitive life on the earth were formed in the space and delivered to the earth.

### References

- [1] Elisila J.E., Glavin D.P., Dworkin J.P. (2009) Cometary glycine in samples returned by stardust. *Meteoritics & Planetary Science* 44, 1323-1330
- [2] Cronin J.R. and Pizzarello S. (1983) Amino acid in meteorites. *Advances in space research* 3, 5-18
- [3] Greenberg J.M., Aigen Li (1997) Silicate core-organic refractory mantle articles as interstellar dust and as aggregates in comets and stellar disks. *Advance in space research* 19, 981-990
- [4] Blank J.G., Millar G.H., Michael J.A., Winas R.E. (1999) Experimental shock chemistry of aqueous amino acid solution and cometary delivery of periodic compounds. *Origin of Life and Evolution of the Biosphere* 31, 15-51

Keywords: comet, amino acid, silica gel, shock compression

## Microtexture and formation mechanism of impact diamonds from the Popigai crater, Russia

OHFUJI, Hiroaki<sup>1\*</sup> ; YAMASHITA, Tomoharu<sup>1</sup> ; LITASOV, Konstantin<sup>2</sup> ; AFANASIEV, Valentin<sup>2</sup> ; POKHILENKO, Nikolai<sup>2</sup>

<sup>1</sup>Geodynamics Research Center, Ehime University, <sup>2</sup>Siberian Branch of the Russian Academy of Sciences

Large meteoritic impact occasionally produces an extensive amount of diamond on the surface of the Earth [1, 2]. Popigai crater located in the north central Siberia is a typical example of such diamond-forming shock events and has recently been brought back into the spotlight due to its vast estimated reserves of the impact diamonds [2-4]. Authigenic impact diamonds occur in shocked graphite-bearing garnet-biotite gneisses that are found as inclusions in impact melt rocks, so-called tagamites and suevites. Popigai diamonds occur as irregular to tabular grains of 0.5-2 mm size (up to 10 mm) and usually show yellow, gray or black colors [3]. Electron microscopic (SEM and TEM) observations in previous studies described that they are polycrystalline aggregates of 0.1-1  $\mu\text{m}$  grains and show a distinct preferred orientation along the [111], which is in a coaxial relation to the [001] of the original graphite source [2-4]. This crystallographic feature as well as the occasional coexistence of lonsdaleite, a metastable carbon polymorph, suggest the Martensitic phase transformation for the potential formation process of the impact diamonds from Popigai crater. However, the textural feature of the impact diamonds and its variation has not fully been examined. Here, we present the result of detailed microtextural observations of impact diamonds from the Popigai crater by transmission electron microscopy (TEM) and discuss the formation mechanism and condition in comparison with those of synthetic diamonds obtained by high pressure and high temperature experiments.

In total 10 diamond grains (7 transparent yellowish and 3 black samples) from the Popigai crater were studied. Each sample was first analyzed by a micro-focus XRD equipped with a Mo target and an IP detector. The results showed that transparent samples consist mostly of diamond and occasionally contain lonsdaleite, while black ones are a mixture of graphite, lonsdaleite and diamond, which are all in a coaxial relation as shown by 2D diffraction patterns collected in transmission geometry. Each sample was then transferred to a focused ion beam (FIB) system to cut out TEM foil sections perpendicular to the surface (of the tabular grains). TEM observation revealed that although all the samples commonly possess layered structures and preferred orientation (mostly along [111] of diamond), there are varieties in crystallite (grain) size (down to 10-20 nm) and degree of preferred orientation. Taking into account the similarity in texture and preferred orientation feature between the Popigai diamonds and synthetic diamond, the variation is likely derived from the small difference in crystallinity of the starting graphite sources and perhaps more significantly from the difference in shock temperature.

According to the shock features recorded in the silicate minerals of the diamond-bearing impactites, the threshold pressure for the onset of the graphite-diamond transformation is estimated to be 34-36 GPa [3]. However, our recent experimental synthesis [5] demonstrated that a similar phase assembly (mostly diamond + traces of lonsdaleite) and microtexture can be produced at much lower pressures of 15-25 GPa at  $>2000$  °C. The shock pressure as well as shock- and post-shock temperature accompanied with the formation of the Popigai crater might be needed to be reevaluated carefully to understand the real nature of the giant impact.

- [1] Masaitis V.L. (1998) *Meteoritics & Planetary Science*. 33. 349-359.
- [2] Langenhorst F., Shafranovsky G.I., et al. (1999) *Geology*. 27. 747-750.
- [3] Deutsch A., Masaitis V.L., et al. (2000) *Episodes*. 23. 3-11.
- [4] Koeberl C., Masaitis V.L., et al. (1997) *Geology*. 25. 967-970.
- [5] Isobe F., Ohfuchi H., et al. (2013) *Journal of Nanomaterials*. 2013. 380165.

## Melting and crystal growth textures developed in rapid heating and cooling of olivine fine particles

ISOBE, Hiroshi<sup>1\*</sup> ; GONDO, Takaaki<sup>1</sup>

<sup>1</sup>Grad. Sch. Sci. Tech., Kumamoto Univ.

Olivine is one of the most common mineral in the solid Earth and chondritic meteorites. Olivine crystals show characteristic textures in chondrules depending on heating and cooling histories in chondrule formation processes at the early solar system. In this study, quick heating and cooling experiments of mixed olivine particles were carried out with a fine particles free falling apparatus (Isobe and Gondo, 2013). In the run products, characteristic melting and crystal growth textures controlled by phase relations, diffusion, and nucleation and growth behavior of olivine can be seen.

Starting material is mixed powder of natural olivine (Fo90), fayalite and an artificial olivine (Fo55). The typical diameter of the starting material particles is approximately 100 micron meters. Each particle is single crystal of olivine or mixture of two or three kinds of raw materials. Heating and cooling experiments are carried out in a high temperature furnace with mass flow controllers to regulate oxygen fugacity and total gas flow rate. Particles can be heated to 1400 degrees C within two seconds, are kept over 1400 degrees C approximately one second and quenched within a second. Maximum temperature has negative correlation to diameter of the particles, and cooling rate has positive correlation to the diameter depending on the falling velocity of the particles. Run products show spherical shape when the particles mostly melted, and are crystal fragments when the particles did not melt. The outside shape of the retrieved run products are observed with a scanning electron microscope. Inner textures of the particles are observed on polished section of the particles. Chemical compositions are also analyzed on the sections.

Fayalite grains are completely melted and Fo90 olivine grains are not melted by themselves concordantly with the phase relation of olivine. Internal textures of Fo55 olivine crystals show quick partial melting when the temperature reach solidus temperature. In the mixed olivine particles, relict crystals of Fo90 and Fo55 olivines dissolve to iron-rich melt derived from melting of fayalite. The dissolution of relict crystals produce steep chemical gradient at interface between crystals and melt.

Run products like barred olivine chondrules or melted cosmic spherules are produced from completely melted particles. In the particles including relict crystals, overgrowth textures from the relict crystals can be seen. Dendritic olivine crystals with regulated crystallographic orientation are developed in melted particles. Surface texture of melted particles may be affected by the dendritic olivine crystals. Oriented magnetite dendrites may also occur between olivine crystals when oxygen fugacity was in the magnetite stability field. Melting, nucleation and crystal growth processes in a few seconds can be discussed from the textures in the run products.

Keywords: Olivine, chondrule, nucleation, crystal growth, dendrites, quench texture

## Temperature-dependent thermal expansivities of aluminum-free silicate melts and borosilicate melts

SUGAWARA, Toru<sup>1\*</sup>; KATSUKI, Junki<sup>2</sup>; YOSHIDA, Satoshi<sup>2</sup>; MATSUOKA, Jun<sup>2</sup>; MINAMI, Kazuhiro<sup>3</sup>; OCHI, Eiji<sup>3</sup>

<sup>1</sup>Akita University, <sup>2</sup>The University of Shiga Prefecture, <sup>3</sup>Japan Nuclear Fuel Limited

Thermal expansivities ( $dV/dT$ ) of silicate melts are essential in a thermodynamic calculation of phase equilibria in magmatic system as a function of pressure and temperature and in a numerical simulation of flow and thermal structures in glass melting furnace. Previous studies have been suggested that the  $dV/dT$  of aluminosilicate melts (Lange, 1996; Potuzak et al., 2006) and magmatic silicate melts (Lange, 1997; Ghiorso and Kress, 2004) is a function of composition, but independent of temperature. On the other hand, it has been reported that the  $dV/dT$  of  $SiO_2$ - $TiO_2$ - $Na_2O$  melt (Liu and Lange, 2001) and  $50SiO_2$ - $25CaO$ - $25MgO$  melt (Gottsmann and Dingwell, 2000) decrease with increasing temperature. Recently, we found that simulated-radioactive waste glass melt which has sodium-borosilicate composition also shows negative temperature-dependent  $dV/dT$  (Sugawara et al., 2013). We carried out density measurements for sodium-silicate melts ( $(100-x)SiO_2$ - $xNa_2O$ ,  $x=23$  or  $32.3$  mol%), commercial soda-lime silicate melt ( $71SiO_2$ - $6MgO$ - $9CaO$ - $14Na_2O$ , mol%) and borosilicate melts ( $66.6SiO_2$ - $yB_2O_3$ - $(33.33-y)Na_2O$  where  $y=8.3, 16.6, 25$ ;  $66.6SiO_2$ - $(12.5+z)B_2O_3$ - $(4.2-z)Al_2O_3$ - $zCaO$ - $(16.7-z)Na_2O$  where  $z=0$  or  $4.2$  mol%). The temperature and compositional dependences of the  $dV/dT$  are discussed based on the new density data and the literature data.

The high-temperature density (dHT) measurement has been made by double-bob Archimedean method between 1173K and 1665K. The glass samples were annealed around glass transition temperature ( $T_g$ ) for 6-396 hours and quenched. Then the density of annealed glasses at 298K (d298) and linear thermal expansivity (dL/L) were determined by Archimedean method and TMA, respectively. The densities of supercooled melt around  $T_g$  (dTg) were calculated from the d298 and the dL/L of glasses. Then, molar volume as a function of temperature and the  $dV/dT$  of melts were obtained by combining the dTg and the dHT.

The  $dV/dT$  values of all samples examined in this study show negative temperature dependence. In the sodium silicate melts, the temperature dependence of the  $dV/dT$  is remarkable when the  $SiO_2$  content increases from 50 to 67 mol%, while the  $dV/dT$  becomes close to zero as further increase in the  $SiO_2$  content. The negative temperature-dependent  $dV/dT$  observed in the  $71SiO_2$ - $6MgO$ - $9CaO$ - $14Na_2O$  melt can be reproduced by an additive sum of the  $dV/dT$  of  $67.8SiO_2$ - $32.2Na_2O$ , diopside (Gottsmann and Dingwell, 2000) and wollastonite (Potuzak et al., 2006) melts. High-temperature Raman spectroscopy for the  $SiO_2$ - $Na_2O$  and  $SiO_2$ - $Na_2O$ - $MgO$  melts has been indicated that amount of Q4 species increases with increasing temperature and  $SiO_2$  and  $MgO$  contents (Maehara et al., 2004, 2005). Therefore, the temperature dependent  $dV/dT$  for the sodium-silicate, commercial soda-lime silicate and diopside melts can be rationalized by an increase of rigid Q4 species at high temperature. The temperature dependence of the  $dV/dT$  is most remarkable in the  $66.6SiO_2$ - $8.3B_2O_3$ - $25Na_2O$  melt among the borosilicate melts. The  $dV/dT$  decreases with replacement of  $Na_2O$  by  $B_2O_3$  or  $CaO$  and of  $B_2O_3$  by  $Al_2O_3$ , suggesting that partial molar  $dV/dT$  of  $B_2O_3$  depends on temperature-induced coordination change of boron and their composition dependence (Wu and Stebbins, 2010).

Acknowledgements: This work was a part of the research supported by Japan Nuclear Fuel Limited with Grant-in-Aid by the Ministry of Economy, Trade and Industry.

Keywords: silicate melt, thermal expansivity, densitometry

## Thermodynamic properties of Mg-postperovskite with $\text{Fe}^{3+}$ and $\text{Al}^{3+}$ dopant: an internally consistent LSDA+U study

WANG, Xianlong<sup>1\*</sup> ; TSUCHIYA, Taku<sup>1</sup>

<sup>1</sup>GRC, Ehime University and ELSI, Tokyo Institute of Technology

Thermodynamic properties of  $\text{MgSiO}_3$  perovskite (Pv) and postperovskite (PPv) with Fe and Al incorporation at high pressure and high temperature are important to understand the Earth's lower mantle (LM). The thermodynamic properties of  $\text{Fe}^{2+}$ ,  $\text{Fe}^{3+}$ , and  $\text{Al}^{3+}$ -bearing Pv[1,2,3] and  $\text{Fe}^{2+}$ -bearing PPv[4] have been investigated in our previous works uniformly based on first-principles method combined with the internally consistent LSDA+U method and quasi-harmonic approximation (QHA). However, to date, effects of trivalent ions,  $\text{Fe}^{3+}$  and  $\text{Al}^{3+}$ , on the thermodynamic properties of PPv are still unclear. In this work, by using the same methods with previous works, the structural, electronic, magnetic, and thermodynamic properties of  $(\text{Mg},\text{Fe}^{3+})(\text{Si},\text{Fe}^{3+})\text{O}_3$  and  $(\text{Mg},\text{Fe}^{3+})(\text{Si},\text{Al}^{3+})\text{O}_3$  PPv at several pressures, from 0 GPa to 180 GPa, are investigated. Our results show that for  $(\text{Mg},\text{Fe}^{3+})(\text{Si},\text{Fe}^{3+})\text{O}_3$  PPv,  $\text{Fe}^{3+}$  ions substituted at Mg and Si site respectively have the high and low spin state within the deep LM pressure range, while  $\text{Fe}^{3+}$  in  $(\text{Mg},\text{Fe}^{3+})(\text{Si},\text{Al}^{3+})\text{O}_3$  PPv remains in the high spin state. Furthermore, separated phase between  $\text{Fe}_2\text{O}_3$  and  $\text{Al}_2\text{O}_3$  in PPv is found unfavorable.

### References:

- [1] Metsue, A. and Tsuchiya, T. (2012) *Geophys. J. Int.* **190**, 310.
- [2] Tsuchiya, T. and Wang, X. (2013) *J. Geophys.* **118**, 83.
- [3] Wang, X. and Tsuchiya, T. To be submitted.
- [4] Metsue, A. and Tsuchiya, T. (2011) *J. Geophys. Res.* **116**, B08207.

Keywords: First-principles method, Internally consistent LSDA+U, Thermodynamic properties, Postperovskite

## Thermal expansion of $\text{Ca}(\text{OD})_2$ at high pressure

NAGAI, Takaya<sup>1\*</sup> ; SANO, Asami<sup>2</sup> ; IIZUKA, Riko<sup>3</sup> ; KAGI, Hiroyuki<sup>3</sup> ; HATTORI, Takanori<sup>4</sup>

<sup>1</sup>Faculty of Science, Hokkaido University, <sup>2</sup>Japan Atomic Energy Agency, <sup>3</sup>Graduate School of Science, The University of Tokyo, <sup>4</sup>Materials and Life Science Division, J-PARC Center

$\text{Ca}(\text{OH})_2$  is one of the important hydrous minerals to understand structural behavior at high pressure and high temperature, because this type of structure is a building unit in more complex hydrous phases such as chondrodite. It is surprising that only a few previous researches can be found on crystallography of  $\text{Ca}(\text{OH})_2$  in the conditions of simultaneously high pressure and high temperature. We gave an oral presentation about some preliminary results in this conference last year. We have continued to analyze the data carefully and will add some new information.

Deuterated samples were prepared via hydrothermal treatment with CaO fine powders and excess  $\text{D}_2\text{O}$  water in a Teflon lined stainless steel autoclave at 493 K for 4 days. After the hydrothermal treatment was completed, precipitates were filtered out, washed with  $\text{D}_2\text{O}$  water, and then dried at 383 K under vacuum for 3 hours. The products were confirmed to have the  $\text{CdI}_2$ -type structure by conventional powder X-ray diffraction measurements and were checked to be deuterated by IR absorption spectra. Synchrotron X-ray diffraction experiments were performed at the beamline AR-NE5C, KEK, Japan in order to obtain cell parameters of  $\text{Ca}(\text{OD})_2$  at various P-T conditions from 2-4 GPa and 300-800 K. TOF neutron powder diffraction measurements of  $\text{Ca}(\text{OD})_2$  were carried out from 300 to 773 K at high pressure at the PLANET beamline in J-PARC, Japan. Pressure was estimated by comparing unit cell parameters with those obtained by synchrotron experiments.

All our TOF data obtained include only  $\text{Ca}(\text{OD})_2$  peaks and no peaks from sample surrounding materials such as  $\text{ZrO}_2$  pressure medium, graphite furnace and WC anvils could be detected owing to radial collimators equipped with the 6-ram pressure apparatus (Atsuhime). The detailed structure parameters such as lattice parameters and atomic coordinates could be reasonably refined by the Rietveld method by using a program GSAS. It is an interesting result that thermal expansion along the *c*-axis seems to be suppressed at high pressure comparing to that at ambient pressure. Mechanism of the thermal expansion of  $\text{Ca}(\text{OD})_2$  at high pressure will be discussed.

Keywords: portlandite, thermal expansion, high pressure, synchrotron X-ray diffraction, TOF neutron diffraction

## High-temperature heat capacity of SiO<sub>2</sub>-Al<sub>2</sub>O<sub>3</sub>-RO (R=Mg, Ca, Sr, Ba) melts

SUGAWARA, Toru<sup>1\*</sup>

<sup>1</sup>Akita University

Heat capacity ( $C_p$ ) of silicate melts is an important property in consideration of phase equilibria in magmatic system and a numerical simulation of flow and thermal structures in glass melting furnace. Heat capacity of aluminum-free melts can be expressed by an additive function of partial molar heat capacities for components (Richet and Bottinga, 1985). On the other hand, it has been reported that the heat capacities of aluminosilicate melts show complicated dependence on both temperature and composition (Richet and Mysen, 2005). However, they are still poorly understood due to the lack of calorimetric data. This study provides new experimental data for the high-temperature heat capacities of Ca, Sr and Ba-bearing aluminosilicate melts.

Drop calorimetry measurements were performed for 50SiO<sub>2</sub>-25Al<sub>2</sub>O<sub>3</sub>-25CaO (An), 36.5SiO<sub>2</sub>-27Al<sub>2</sub>O<sub>3</sub>-36.5CaO (Ca36.5), 8SiO<sub>2</sub>-30Al<sub>2</sub>O<sub>3</sub>-62CaO (Ca62) and 75SiO<sub>2</sub>-12.5Al<sub>2</sub>O<sub>3</sub>-12.5SrO or 12.5BaO (Sr12.5, Ba12.5) melts between 873K and 1889K using a Bunsen ice calorimeter. Heat capacity of melts was determined from the differential of measured relative enthalpy. The heat capacity of anorthite melt is  $1.356+0.0001151T(K)$  (J/K-g), which is consistent with the value reported by Richet and Bottinga (1985). The heat capacities for Ca36.5, Ca62, Sr12.5 and Ba12.5 are 1.532, 1.508, 1.313 and 1.160 (J/K-g), respectively, and they are independent of temperature.

The temperature and compositional dependence of the  $C_p$  for SiO<sub>2</sub>-Al<sub>2</sub>O<sub>3</sub>-RO (R=Mg, Ca, Sr, Ba) melts are considered by combining new calorimetric data and literature data by drop calorimetry (n=11, Richet and Bottinga, 1984; Courtial and Richet, 1993; Neuville and Richet, 1991; Richet and Neuville, 1992) and by differential scanning calorimetry (n=22, Webb, 2008, 2011). The positive temperature dependence is observed in the SiO<sub>2</sub>-Al<sub>2</sub>O<sub>3</sub>-MgO melts as reported by Courtial and Richet (1993). In the system SiO<sub>2</sub>-Al<sub>2</sub>O<sub>3</sub>-CaO, temperature dependence of the  $C_p$  is only observed at anorthite composition. The heat capacity of alkaline-earth aluminosilicate melts can be expressed by a symmetric solution model. The derived heat capacity of mixing is negative value in all of the systems. At constant temperature and oxide ratio, the heat capacity decreases with decreasing field strength of alkaline-earth elements (Ba < Sr < Ca < Mg), suggesting that configurational freedom is restricted in the cations with lower field strength due to the charge compensation effect of aluminum. Further experimental data for Sr and Ba-bearing melts are required to generalize temperature dependence of the heat capacity.

Keywords: Silicate melt, Heat capacity, Calorimetry

## Viscosity of titanium-bearing silicate melts at high pressure

SUZUKI, Akio<sup>1\*</sup>

<sup>1</sup>Tohoku University

Knowledge about viscosity of silicate melt is valuable for understanding the activity of magma in the planetary interiors. The high-Ti magmas erupted on the lunar surface. These magmas contains TiO<sub>2</sub> up to 16 wt%. Because the viscosity change at high pressure is affected by the structural change of TO<sub>4</sub>-network, it is very interesting to know the influence of Ti on the pressure dependence of viscosity. We performed viscosity measurement of K<sub>2</sub>TiSi<sub>4</sub>O<sub>11</sub> melt as an analogue of the lunar high-Ti magmas. Viscosity was measured by the falling sphere method using an X-ray radiography system. Experiments were performed at the NE7A station of the PF-AR synchrotron radiation facility in KEK, Tsukuba, Japan. We found that the viscosity of K<sub>2</sub>TiSi<sub>4</sub>O<sub>11</sub> melt has a viscosity minimum at 3 GPa. Paris et al. (1994) reported that the coordination number of titanium increases with increasing pressure on the basis of the XANES spectra of glasses synthesized under high pressure. Our results suggest that the viscosity minimum of K<sub>2</sub>TiSi<sub>4</sub>O<sub>11</sub> is strongly related to the coordination change of titanium. The viscosity minimum is also found in the terrestrial MORB magma. Recently, Sakamaki et al. (2013) proposed that the viscosity minimum causes the low velocity zone of seismic wave in the upper mantle. The present study suggests that the high-Ti melt causes an attenuating zone in the deep lunar mantle.

Keywords: magma, viscosity, moon, mantle

## Study of physical properties of Fe-Si alloy at high pressure using synchrotron radiation Mossbauer spectroscopy

SUZUKI, Nanami<sup>1\*</sup> ; OHTANI, Eiji<sup>1</sup> ; HIRAO, Naohisa<sup>2</sup> ; KAMADA, Seiji<sup>1</sup> ; HAMADA, Maki<sup>3</sup> ; SAKAMAKI, Tatsuya<sup>1</sup> ; OHISHI, Yasuo<sup>2</sup> ; MASUDA, Ryo<sup>4</sup> ; MITSUI, Takaya<sup>5</sup>

<sup>1</sup>Department of Earth and planetary materials science, Graduate School of Science, <sup>2</sup>Japan Synchrotron Radiation Research Institute, Hyogo, 679-5198, Japan, <sup>3</sup>School of Natural System, College of Science and Engineering, Kanazawa University, Kanazawa, 920-119, <sup>4</sup>Research Reactor Institute, Kyoto University, Osaka, 590-0494, Japan, <sup>5</sup>Japan Atomic Energy Agency, Hyogo, 679-5148, Japan

The Earth's core is divided into the liquid outer core and solid inner core based on seismological observations. The Earth's core has been geochemically and cosmochemically thought to be mainly composed of Fe. The density of the core is smaller than that of pure iron under the core conditions. Therefore, the core has been considered to contain light elements, such as H, S, Si, C, and O. Si is one of the most important light elements in the core. Although the phase relations and compression behaviors in the Fe-Si alloy have been studied at high pressure and temperature in order to investigate properties of the inner core, magnetic properties of the alloys have not been studied well. In order to clarify the relationship between the magnetic transition and the structural transition of the Fe-Si alloy, we made simultaneous measurements of X-ray diffraction and synchrotron Mössbauer spectroscopy of the Fe-Si alloy up to 40 GPa at room temperature.

The Fe-Si alloy used for the measurements has a composition of Fe<sub>0.95</sub>Si<sub>0.05</sub> enriched with <sup>57</sup>Fe. The starting material was synthesized by melting the mixture of <sup>57</sup>Fe and Fe-Si alloys under the Ar-H<sub>2</sub> atmosphere by laser heating. Mössbauer spectra and XRD patterns were obtained at the beamlines, BL10XU and BL11XU of SPring-8 up to 40 GPa at room temperature. Our Mössbauer data together with X-ray diffraction data revealed that the magnetic transition from magnetic to non-magnetic phase occurs at 18 GPa simultaneously with the bcc to hcp transition. The change in the sound velocity and compression behavior of the Fe-Si alloy has been reported associated with the structural transformation of the alloy from bcc to hcp. The present results imply that the change in these physical properties is caused not only by the structural change but also by the magnetic transition.

## Experimental determination of post-spinel transition boundary in $\text{Fe}_2\text{SiO}_4$

MATSUZAWA, Taisuke<sup>1\*</sup> ; KOJITANI, Hiroshi<sup>1</sup> ; AKAOGI, Masaki<sup>1</sup>

<sup>1</sup>Department of Chemistry, Gakushuin University

It is widely accepted that  $(\text{Mg,Fe})_2\text{SiO}_4$  ringwoodite is the most abundant mineral in the mantle transition zone. Because spinel-type  $\text{Fe}_2\text{SiO}_4$  is the endmember of  $(\text{Mg,Fe})_2\text{SiO}_4$  ringwoodite, many investigators have been studied on phase transitions of  $\text{Fe}_2\text{SiO}_4$  spinel (Kawada 1977, Ohtani 1979, Morooka 1992, Katsura et al. 1998). Spinel-type  $\text{Fe}_2\text{SiO}_4$  decomposes into  $2\text{Fe}_x\text{O} + \text{SiO}_2$  (stishovite) +  $2(1-x)\text{Fe}$  above about 18GPa. However, the dissociation boundary has not yet been established well due in part to difficulty in oxygen fugacity control. In this study, we determined the post-spinel phase boundary in  $\text{Fe}_2\text{SiO}_4$  by high-pressure experiments controlling oxygen fugacity with the Fe-FeO buffer.

A starting material of high-pressure experiments was a mixture of  $\text{Fe}_2\text{SiO}_4$  (fayalite),  $\text{Fe}_x\text{O}$  and Fe with molar ratios of 10:2:1, and it was packed in a Fe capsule. Oxygen fugacity of the sample at high pressure and high temperature was controlled by the Fe-FeO buffer. The high-pressure experiments were performed using a Kawai-type 6-8-type multi-anvil apparatus at 16-20GPa and 1000-1400 °C. The starting samples were heated at the desired conditions for 3-6 hours, and then quenched and decompressed to ambient conditions. Recovered samples were identified by using powder XRD method and SEM-EDS, and then lattice parameters of  $\text{Fe}_x\text{O}$  were determined by using powder XRD. The x values in  $\text{Fe}_x\text{O}$  were estimated from the composition-lattice parameter relationship of  $\text{Fe}_x\text{O}$  by McCammon (1993).

The post-spinel transition boundary in  $\text{Fe}_2\text{SiO}_4$  was determined to be  $P(\text{GPa}) = -0.0021T(^{\circ}\text{C}) + 20.0$  in the temperature range of 1000-1400 °C. The phase boundary has a negative slope. Our boundary is almost consistent with those of Ohtani (1979) and Katsura et al. (1998). Katsura et al. (1998) interpreted that the negative slope of the boundary in the previous studies was apparent which was caused by slow kinetics of spinel decomposition. Because our study indicated that the decomposition of  $\text{Fe}_2\text{SiO}_4$  spinel completed in the runs for 3 hours at 1000 °C and that x values of  $\text{Fe}_x\text{O}$  in the run products for 3 and 6 hours at the 1000 °C were approximately equal, we conclude that heating at 1000 °C for at least 3 hours was enough to reach the equilibrium. Because our transition boundary was determined by the runs for 6 hours at 1000 °C, 3 hours at 1200 °C, and 3 hours at 1400 °C, we suggest that the negative slope of the post-spinel transition boundary in  $\text{Fe}_2\text{SiO}_4$  is not apparent but the essential feature.

Keywords:  $\text{Fe}_2\text{SiO}_4$ , post-spinel, spinel, high-pressure

## Relationship between Raman spectral pattern and crystal orientation of cordierite

ABE, Miyako<sup>1\*</sup> ; MADHUSOODHAN, Satish-kumar<sup>1</sup> ; KAGI, Hiroyuki<sup>2</sup>

<sup>1</sup>Niigata University, <sup>2</sup>Tokyo University

In the crystal structure of cordierite, six-membered rings of (Al, Si) O<sub>4</sub> are stacked along the *c*-axis and form a channel structure. This channel structure can trap volatiles such as H<sub>2</sub>O and CO<sub>2</sub>, and makes cordierite an important mineral for preserving the information of past fluid conditions during metamorphism. Earlier studies have shown that the intensity of CO<sub>2</sub> Raman band represents the contents of CO<sub>2</sub> inside the channel (e.g. Kaindl et al., 2006). Carbon dioxide is aligned linearly along the *a*-axis in the channel (Aines and Rossman, 1984), and therefore the peak intensity of CO<sub>2</sub> at 1383cm<sup>-1</sup> in the Raman spectra varies considerably depending on the crystal orientation of cordierite (Kolesov and Geiger, 2000). Thus, it is necessary to correct the effect of crystal orientation for the determination of true contents of CO<sub>2</sub> in randomly oriented cordierite grains in metamorphic rocks. As a first step to accurately quantify the CO<sub>2</sub> content in cordierite using Raman spectroscopy, we analyzed euhedral crystals of cordierite for revealing the relationship between Raman spectral patterns and crystal orientation.

In this study, euhedral cordierite crystals collected from the volcanic ash deposit in the Takiga swamp, Gunma Prefecture, Japan were examined in detail using micro-Raman spectroscopy. Raman spectra were observed with different conditions for each analytical point to check the effect of polarization and crystal orientation. Mineral chemical analyses of cordierite crystals indicate homogeneity in its composition ( $X_{Mg} = 0.735 \pm 0.14$ ). However, different Raman spectral patterns were obtained for (001) plane and (100) plane; the (001) plane show only one pattern, but the (100) plane showed three different patterns. Peak splitting between 554 and 575 cm<sup>-1</sup>, the peaks of 970 cm<sup>-1</sup> and 1180 cm<sup>-1</sup> changed its intensity drastically, whereas the peak at 670 cm<sup>-1</sup> remained constant. We selected five Raman peaks at 554 cm<sup>-1</sup>, 575 cm<sup>-1</sup>, 670 cm<sup>-1</sup>, 970 cm<sup>-1</sup>, and 1180 cm<sup>-1</sup> attributable to the cordierite (Al, Si)O<sub>4</sub> structure and analyzed the intensity ratio of these five peaks in different orientations. A parameter of  $\Delta$ intensity was defined, where the intensity ratios of (001) plane were concentrated around 0, and those of (100) plane deviates from 0. This parameter can be used to identify the crystal orientation of cordierite. The spectral variations observed in cordierite and its relationship with crystal orientation are interpreted based on the stretching and/or bending vibrations of cordierite unit cell structure

Keywords: Cordierite, Raman spectroscopy, Crystal orientation

References

Aines, R. D. and Rossman, G. R. (1984) The high temperature behavior of water and carbon dioxide in cordierite and beryl. *American Mineralogist*, 69, 319-327

Kaindl, R., Tropper, P. and Deibl, I. (2006) A semi-quantitative technique for determination of CO<sub>2</sub> in cordierite by Raman spectroscopy in thin sections. *European Journal of Mineralogy*, 18, 331-335

Kolesov, B. A. and Geiger, C. A. (2000) Cordierite II: The role of CO<sub>2</sub> and H<sub>2</sub>O. *American Mineralogist*, 85, 1265-1274

Keywords: Cordierite, Raman spectroscopy, Crystal orientation

## The low-temperature Moessbauer spectroscopy of an M3' epidote from Osayama, Okayama prefecture, Japan

YAMAKAWA, Junji<sup>1\*</sup>; KAWASE, Masaya<sup>2</sup>; KUROKUZU, Masayuki<sup>3</sup>; MORIMOTO, Shotaro<sup>4</sup>; SAITO, Tadashi<sup>5</sup>

<sup>1</sup>Graduate School of Natural Science and Technology, Okayama University, <sup>2</sup>Nagahama Institute of Bio-Science and Technology, <sup>3</sup>Research Reactor Institute, Kyoto University, <sup>4</sup>Faculty of Pharmacy, Osaka Ohtani University, <sup>5</sup>Radioisotope Center, Osaka University

Epidote,  $\text{Ca}_2(\text{Al,Fe}^{3+},\text{Fe}^{2+})\text{Al}_2\text{SiO}_4\text{Si}_2\text{O}_7(\text{O,OH})$  is a common rock forming mineral found low-grade metamorphic rocks. The chemical compositions of the epidote vary with the formation conditions and make some complex zoning textures. The distribution of  $\text{Fe}^{2+}$ - $\text{Fe}^{3+}$  ions in the crystal structure will be able to analyze by the Mössbauer spectrometry and the stability/unstability of the sample can be estimated from the distribution.

Moreover, in some sample, the Fe ions are distributed in the characteristic M3' site that can be detected by the Mössbauer spectroscopy. The distribution ratio of the Fe ions in the M3' site can not be estimated by the X-ray structure analysis, so the M3' sites are making a small ordering structures and distribute homogeneously in the crystal. Distribution ratio of Fe in the site of M1/M3/M3' corresponds to the formation conditions of the sample.

In this study, the low-temperature Mössbauer spectrum and Magnetic susceptibility of the M3' epidote sample was measured and the characteristics of the M3' site were analysed.

Keywords: Epidote, Moessbauer spectroscopy, M3' site, Magnetic susceptibility

## Structural change in ikaite ( $\text{CaCO}_3 \cdot 6\text{H}_2\text{O}$ ) near the freezing point temperature of water

TATENO, Natsuki<sup>1</sup> ; KYONO, Atsushi<sup>1\*</sup>

<sup>1</sup>Div of Earth Evolution Sciences, Grad Sch of Life & Environmental Sciences, Univ of Tsukuba

Ikaite, one of the calcium carbonate minerals, is thermodynamically stable only at near-freezing temperature and transformed rapidly into calcite and vaterite at ambient temperature. During the phase transformation with dehydration, its crystal shape is preserved as pseudomorphs, termed glendonite, thinolite, and gennoishi. This study aims to clarify the structure change and dehydration mechanisms by using low-temperature single-crystal X-ray diffraction study. At  $-50$  °C, the crystal structure of ikaite is monoclinic, space group  $C2/c$  with the unit cell parameter  $a = 8.8134$  (1),  $b = 8.3108$  (1),  $c = 11.0183$  (1) Å,  $\beta = 110.418$  (1) °. It is composed of four  $\text{CaCO}_3 \cdot 6\text{H}_2\text{O}$  molecules in the cell. With increasing temperature, the unit cell volume is increased monotonously from  $756.3$  to  $758.0$  Å<sup>3</sup> between  $-50$  and  $-20$  °C, and then jumped to  $771.0$  Å<sup>3</sup> at  $-10$  °C. The unit cell lattice anisotropically expands mainly along the  $c$ -axis, followed by the  $a$ -axis. The intramolecular Ca-O(5) bond distance is drastically elongated at  $-10$  °C, which is associated with elongations of the intermolecular O(2)-O(3), O(2)-O(5), O(4)-O(5) distances. The  $a$  unit cell expansion is directly due to the elongation of the O(2)-O(5) aligned parallel to the  $a$ -axis. The drastic elongation of the Ca-O(5) bond distance gives rise to an initial dehydration of the  $\text{CaCO}_3 \cdot 6\text{H}_2\text{O}$  molecule. The intermolecular Ca-O(3)-O(2) angle is constantly increased with temperature, leading to rotational motion of the  $\text{CaCO}_3 \cdot 6\text{H}_2\text{O}$  molecule along  $b$ -axis. This is responsible for the highest expansion coefficient of the  $c$  lattice parameter.

Keywords: ikaite, vaterite, calcium carbonate, pseudomorph, low-temperature X-ray diffraction study

## Synchrotron powder X-ray diffraction study of the structural thermal properties on hydrogrossular

KATO, Masato<sup>1\*</sup> ; KYONO, Atsushi<sup>2</sup>

<sup>1</sup>Graduate School of Life and Environmental Science, <sup>2</sup>Graduate School of Life and Environmental Science

Synchrotron powder X-ray diffraction study on synthetic Si-free hydrogrossular, katoite  $\text{Ca}_3\text{Al}_2(\text{O}_4\text{H}_4)_3$ , were performed at temperature range from 300 to 10 K. The temperature dependence of structure parameters was refined by Rietveld analysis. Since structural contraction with decreasing temperature would directly cause a phase transition on the hydrogrossular structure, three candidates for space group:  $Ia-3d$  (katoite at ambient),  $I-43d$  (katoite at high pressure), and  $I4_1/acd$  (majorite), were applied to the X-ray diffraction profile fitting collected at 10 K. The final  $R_w$  with the  $Ia-3d$  space group consequently results in the smallest value, which suggests that the katoite structure remains unchanged up to the lowest temperature of 10 K. However, the temperature dependence of the unit cell volume shows two different expansion coefficients at temperatures above and below 100 K. It can be accounted for by the effect of the repulsion between atoms of the same species. Whereas the unit cell of katoite is monotonously contracted with decreasing temperature, the  $\text{O}_4\text{H}_4$  tetrahedron and  $\text{AlO}_6$  octahedron are alternatively expanded and contracted. Compared with the phase transition in katoite under high pressure, moreover, the unit cell volume contraction up to 5 GPa is about eight times larger than that under low temperature. The structural characteristics could therefore explain the reason why no phase transition occurs in katoite at low temperature condition.

Keywords: katoite, synchrotron powder X-ray diffraction, Rietveld analysis,  $\text{O}_4\text{H}_4$  tetrahedron

## Structural study on the phase transformation of natural scolecite with increasing temperature

UCHIDA, Takahiro<sup>1\*</sup>; KURIBAYASHI, Takahiro<sup>1</sup>; NAGASE, Toshiro<sup>2</sup>

<sup>1</sup>Department of Earth Science, graduate school of science, Tohoku University, <sup>2</sup>The Tohoku University Museum, Tohoku University

Scolecite,  $\text{CaAl}_2\text{Si}_3\text{O}_{10}\cdot 3\text{H}_2\text{O}$  is classified to fibrous zeolite group. The sequence of general phase transformation with increasing temperature has been reported for natural scolecite: scolecite  $\rightarrow$  meta-scolecite  $\rightarrow$  amorphous phase and decomposes to An + Qtz (Rykl *et al.* 1986; Gottardi and Galli 1985).

In this study, the high-T evolution of the structure of natural scolecite from Poona, India were studied up to 573 K to reevaluate the dehydration process of scolecite using TG-DTA and in situ single crystal X-ray diffraction experiments.

As the results from structural refinement at room temperature, the lattice constants of the sample are determined as follows :  $a = 18.504(3)\text{Å}$ ,  $b = 18.971(2)\text{Å}$ ,  $c = 6.5262(9)\text{Å}$  and  $\beta = 90.558(5)^\circ$ . The crystal structure of scolecite,  $\text{CaAl}_2\text{Si}_3\text{O}_{10}\cdot 3\text{H}_2\text{O}$ , was refined with the space group  $F1d1$  from 3567 reflections with  $I_o > 2\sigma(I)$ , yielding  $R = 4.62\%$ ,  $wR = 11.41\%$ . At  $\sim 423\text{K}$ , the space group was changed to  $Fd11$  from  $F1d1$ , and scolecite underwent a phase transformation to meta-scolecite phase.

As the results from structural refinement at 523 K, the lattice constants of the sample are determined as follows :  $a = 18.122(3)\text{Å}$ ,  $b = 18.847(3)\text{Å}$ ,  $c = 6.5408(11)\text{Å}$  and  $\alpha = 88.948(7)^\circ$ . The crystal structure of scolecite,  $\text{CaAl}_2\text{Si}_3\text{O}_{10}\cdot 2\text{H}_2\text{O}$ , was refined with the space group  $Fd11$  from 2782 reflections with  $I_o > 2\sigma(I)$ , yielding  $R = 10.72\%$ ,  $wR = 28.85\%$ . When phase transformation occurs, OW2 in scolecite is expelled and then the half of Ca ions move by  $\sim 1/2c$ . At 573 K, the number of observed reflections was decreased dramatically.

Under high-T experiments from 423 to 523 K, two reciprocal lattices were observed, each lattice is corresponding to twin component with the [00-1] twin law. The [00-1] twinning could be associated with the dehydration mechanism. The X-ray diffraction data suggest the possibility of exist of a new  $\text{H}_2\text{O}$  site in meta-scolecite phase. This may be a key to solve the dehydration process of scolecite.

Keywords: scolecite, dehydration, phase transformation, single crystal X-ray diffraction, twin, high temperature

## Near-infrared spectra of ice under high pressure and high temperature

NOGUCHI, Naoki<sup>1\*</sup> ; KOMATSU, Kazuki<sup>2</sup> ; SHINOZAKI, Ayako<sup>2</sup> ; SHINODA, Keiji<sup>3</sup> ; KAGI, Hiroyuki<sup>2</sup>

<sup>1</sup>Graduate School of Engineering, Hiroshima University, <sup>2</sup>Geochemical Laboratory, Graduate School of Science, The University of Tokyo, <sup>3</sup>Department of Geosciences, Faculty of Science, Osaka City University

The physical properties of ice VII under high pressure and high temperature (HP-HT) conditions are important to planetary science. Ice VII is considered a primary constituent of the interior of giant icy satellites and planets (e.g., Podolak et al. 1998). Thus, understanding the physical properties of ice VII will contribute to better knowledge about the structure and dynamics of other satellite and planetary interiors. In particular, the ionic conductivity of ice VII, which affects the magnetic fields of these bodies (Stevenson 2003), is controlled by ionic and rotational defects in the ices (Jaccard 1959); moreover, ionic defects have two types: OH<sup>-</sup> and H<sub>3</sub>O<sup>+</sup>. The probability of forming defects in ice VII under the HP - HT conditions that typify the interiors of icy satellites and planets is surely increased by thermal activation.

In the near-infrared (NIR) region, the spectrum of ice VII shows absorption bands of the bending-stretching combination ( $\nu_2 + \nu_3$ ) and stretching overtone ( $2\nu_3$ ) modes of the normal vibration of water molecules (Larsen and Williams 1998). These modes correspond to the high vibrational energy level of the potential well, and provide information regarding the potential barrier along the O...O axis. To determine the probability of forming ionic defects in the ice VII structure at elevated temperatures, the NIR spectra of ice VII must be measured. The aim of this study is to investigate the state of protons in ice VII under HP-HT conditions. Thus, we measured the NIR absorption spectra of water at pressures up to 16 GPa and temperatures up to 368 °C using an external heating diamond anvil cell and synchrotron NIR radiation of BL43IR at SPring-8.

The absorption band of the first OH stretching overtone mode divided into doublet peaks above 5 GPa at room temperature, suggesting that proton tunneling occurs at the overtone level. As the temperature increased, the doublet peaks gradually reduced to a singlet. This result implies that thermally activated protons hop between the two potential minima along the oxygen-oxygen axis. A P-T diagram for the proton state was constructed from the changing band shape of the overtone mode.

Keywords: ice, proton, icy satellite, near-infrared spectroscopy, high pressure and high temperature

## Phase changes of filled ice Ih methane hydrate induced by the orientational ordering of the guest molecules

TANAKA, Takehiko<sup>1\*</sup> ; HIRAI, Hisako<sup>1</sup> ; MATSUOKA, Takahiro<sup>2</sup> ; OHISHI, Yasuo<sup>3</sup> ; YAGI, Takehiko<sup>1</sup> ; OHTAKE, Michika<sup>4</sup> ; YAMAMOTO, Yoshitaka<sup>4</sup> ; NAKANO, Satoshi<sup>5</sup>

<sup>1</sup>Geodynamics Research Center, Ehime University, <sup>2</sup>Gifu University, <sup>3</sup>Japan Synchrotron Radiation Research Institute, <sup>4</sup>The National Institute of Advanced Industrial Science and Technology, <sup>5</sup>National Institute for Materials Science

Oriental ordering of guest methane molecules in a filled ice Ih structure of methane hydrate (MH) was observed above 15 to 20 GPa at room temperature in a previous Raman study. However, the change in the fundamental structure was not observed at the pressure region by X-ray diffractometry. In this study, low-temperature and high-pressure experiments were performed with filled ice Ih structure of methane hydrate under pressure and temperature conditions of 2.0 to 77.0 GPa and 30 to 300 K, respectively, using diamond anvil cells and a helium-refrigeration cryostat. Distinct changes in the axial ratios of the host framework were revealed by In-situ X-ray diffractometry. Splitting in the CH vibration modes of the guest methane molecules, which was previously explained by the orientational ordering of the guest molecules, was observed by Raman spectroscopy. The pressure and temperature conditions at the split of the vibration modes agreed well with those of the axial ratio changes. The results indicated that orientational ordering of the guest methane molecules from orientational disordered-state occurred at high pressures and low temperatures, and that this guest ordering led to the axial ratio changes in the host framework. Existing regions of the guest disordered-phase and the guest ordered-phase were roughly estimated by the X-ray data. In addition, above the pressure of the guest-ordered phase, another high pressure phase was developed at a low-temperature region.

Keywords: Methane Hydrate, X ray diffraction, high pressure, Raman spectroscopy

## Zirconium local structure in tektite and impact-related natural glasses probed by XAFS

TOBASE, Tsubasa<sup>1\*</sup> ; YOSHIASA, Akira<sup>1</sup> ; WANG, Ring<sup>1</sup> ; HIRATOKO, Tatsuya<sup>1</sup>

<sup>1</sup>Graduate School of Science, Kumamoto University, <sup>2</sup>Materials and Structures Laboratory, Tokyo Institute of Technology

The local structures of tektite and natural glasses were studied by Zr K-edge X-ray absorption near edge structure (XANES) and extended X-ray absorption fine structure (EXAFS) in order to provide quantitative data on bonding distances and coordination numbers. The XAFS measurements were performed at the beam line BL-NW10A of the PF-AR in National Laboratory for High Energy Physics (KEK), Tsukuba, Japan. Zr<sup>4+</sup> ion in tektite has different kinds of coordination environment. Various natural glasses are formed under different physical conditions. Impact-related glass, fulgurite and volcanic glasses are typical natural glasses. Glass structure is affected by the pressure and temperature conditions during the glass formation and annealing process. This study indicated that different formation process of natural glasses gives different local structure of zirconium ions.

The Zr K-edge XANES spectra of tektite have the double post-edge peaks with different heights. All tektites are classified in same types. Zr-O distances in tektite are 2.198-2.215 Å and XANES spectra of tektite have similar shape. It indicates that tektites have similar Zr local structure with 7-fold coordination Zr ions. Volcanic glasses are classified same type. Impact-related glasses are classified to different types. Impact glasses are formed under different geological process at impact event and are experienced different physical environments.

Keywords: XAFS, Local structure of Zr, Tektite, Natural glass, XANES, EXAFS

## Light element quantification using electron microprobe and Os surface coating

OHFUJI, Hiroaki<sup>1\*</sup> ; YAMAMOTO, Masashi<sup>1</sup> ; KOJIMA, Yohei<sup>1</sup>

<sup>1</sup>Geodynamics Research Center, Ehime University

Electron microprobe analysis is a non-destructive method widely used for determining the chemical composition of solid materials such as not only minerals and rocks but also industrial and biological materials. Recent advances of solid-state detectors for energy dispersive spectroscopy (EDS) analysis allow us to readily collect precise quantitative data. For SEM and EDS analysis of non-conductive (insulating) materials such as minerals and rocks, surface coating of a thin conductive layer is a prerequisite for sample preparation. For this purpose, carbon and gold are most commonly used; the former with low atomic (*Z*) number is suitable for microprobe chemical analysis, while the latter is preferable for textural observation of samples with rough, uneven surfaces and/or with high porosity. Recently, osmium coating prepared by chemical vapor deposition (CVD) has been a focus of attention and found to be effective for high-resolution SEM observation of samples with uneven surfaces. In the present study, we applied the sample preparation technique using very thin osmium surface coating for chemical quantification of various mineral samples by EDS.

The SEM-EDS analysis was performed by using FE-SEM (JEOL, JSM-7000F) equipped with a silicon-drift-type EDS detector (Oxford Instruments, X-Max 20). Accelerating voltage and probe current were 15 kV and 1 nA, respectively. Osmium coating of 5 nm thick was carefully made by using a Neoc-ST osmium coater (Meiwafosis). Quantification analyses were conducted on a variety of mineral samples, silicate (including hydrous silicates), carbonate and oxide minerals.

The results showed that the quantification data obtained from samples with osmium coating are as accurate as those from samples with conventional carbon coating for principle elements such as Na, Mg, Al, Si, K, Ca and Fe. With respect to the quantification of light elements such as C, N and O, the results from osmium-coated samples are found to be closer to their stoichiometric values than those from carbon-coated samples. This is likely caused by the absorption correction of the X-rays passing through each coating layer. The thickness of the surface coating layer can be precisely controlled in the case of osmium coating prepared by the CVD technique, but not readily adjusted in carbon coating. As the result, the deviation of the estimated thickness of the coating layer from the actual thickness over/underestimates the effect of X-ray absorption correction, in which low-energy X-rays from light elements are more significantly influenced by the correction. We found that the precise quantification of oxygen as a separate element (not as oxide forms of cations) using osmium surface coating might be helpful and effective in estimation of the valence state of iron in iron-bearing minerals and water (hydrogen) content in hydrous minerals. We also confirmed that the present technique is also useful for precise quantification of carbonate minerals such as CaCO<sub>3</sub>.

## Cathodoluminescence characterization of terrestrial and extraterrestrial alkali-halide minerals

YOSHIDA, Eisuke<sup>1\*</sup>; NISHIDO, Hirotsugu<sup>1</sup>; NINAGAWA, Kiyotaka<sup>1</sup>

<sup>1</sup>Okayama University of Science

Luminescence of natural alkali halides such as halite and sylvite is characterized by structural defects related to F-center (+p) and V-center (+e). On their CL (cathodoluminescence), however, scarcely has been reported so far. Since asteroidal water was discovered as fluid inclusion in halite from H5 chondrite, Monahans (1998), alkali halides in meteorites have been extensively investigated for understandings of aqueous alteration and thermal metamorphism on the parent body. Therefore, luminescence features of halides can provide valuable information on such issues. In this study we have measured CL spectra of terrestrial and extraterrestrial halite samples to clarify luminescence centers in various types of halite.

Halite crystals of terrestrial origin and small halite particles in ureilite meteorites were selected for CL measurements. All samples were prepared using oil while cutting and polishing without water. Also cleavage fragments of terrestrial samples were used for CL spectral measurements after carbon coating.

All samples exhibit weak blue to greenish blue CL with broad band emissions from 350 to 650 nm. CL spectra corrected for total instrumental response were converted into energy units for spectral deconvolution using a Gaussian curve fitting, because Gaussian curve in energy units can be assigned to one specific type of emission center (Stevens-Kalceff, 2009). The deconvoluted components can be assigned to the emission centers related to  $V_k$  (+e), F (+p),  $V_F$  (+e),  $Mn^{2+}$  ( $Na^+$ ) and  $Mn^{2+}$  (interstitial) by referring to Gorobets and Rogojine (2002).

The CL spectra of terrestrial halite at room temperature are consisted of five components at 3.34 eV, 3.05 eV, 2.46 eV, and 2.28 eV and at 2.00 eV. At low temperature the emission of  $Mn^{2+}$  impurity center is enhanced due to an increase in the probability of radiation transition. In the case of high-energy emission, a decrease in sample temperature reduces the intensity of F-center emission, but sensitizes the intensity of  $V_k$ -center emission, suggesting the energy transfer from F-center to  $V_k$ -center. The CL spectral analysis of terrestrial sylvite at room temperature confirms four emission components at 3.32 eV, 2.97 eV, 2.53 eV and 1.89 eV.

Halite in the meteorite of polymict ureilite (Dar al Gani 319) gives a broad emission band in blue region, which is deconvoluted into two components at 2.70 eV for unknown center and at 3.11 eV for F-center. However, no emission in red region associated with Mn impurity center has not recognized in ureilite halite. It implies that high-energy radiation in cosmic space might break up the crystal fields around Mn ions.

## Effects of Mn activator and site occupancy on cathodoluminescence of dolomite

KUSANO, Nobuhiro<sup>1\*</sup>; NISHIDO, Hirotsugu<sup>1</sup>; NINAGAWA, Kiyotaka<sup>1</sup>

<sup>1</sup>Okayama University of Science

Cathodoluminescence (CL) has been widely applied in mineralogical and petrological investigations, especially for carbonates. Dolomite commonly red CL emission related to an impurity center of divalent Mn in Ca-site and Mg-site (Sommer, 1972; Walker et al, 1989). Furthermore, temperature effect on CL efficiency has not been discussed in spite of potentially important function to control CL emission mechanism. In this study we have clarified luminescent mechanism of dolomite in a wide range of temperature using a SEM-CL, and confirmed a temperature quenching of its emissions. The quenching process has been quantitatively evaluated by CL spectral deconvolution method assuming the Mott-Seitz model.

Five dolomite samples from Hase, Japan (D01), Nakase, Japan (D02), Raura, Peru (D03), Binntal, Switzerland (D04), Arizona, USA (D05) were selected for CL measurements after carbon-coating on their polished surfaces. SEM-CL analysis was conducted using an SEM (JEOL:JSM-5410) combined with a grating monochromator (Oxford: Mono CL2) to measure CL spectra ranging from 300 to 800 nm in 1 nm steps with a temperature controlled stage from -190 to 250 °C. The dispersed CL was collected by a photon counting method using a photomultiplier tube (R2228) and converted to digital data. All CL spectra were corrected for the total instrumental response.

CL spectra of all samples at room temperature exhibit almost similar pattern with a broad band at 525-800 nm in a red region. The spectral peaks are sharpened and enhanced at lower temperature due to reduction of thermal lattice vibration and an increase in luminescent efficiency, suggesting high spectral resolution of the emission bands at low temperature. Therefore, a Gaussian fitting was conducted to quantitatively deconvolute spectral data obtained at low temperature in an energy unit. The results confirmed that CL of all samples consist of two emission components at around 1.84 eV (Mg-site) and 2.15 eV (Ca-site) in red region, of which variation might be attributable to crystal field (Mn-ligands distance). In general, luminescence efficiency of the material decreases with a rise in temperature due to an increase in non-radiative transitions. This phenomenon has been recognized in several minerals such as quartz, cristobalite and tridymite as temperature quenching. Furthermore, an increasing temperature makes a shift of the emission peak to a higher wavelength side. The emission intensity varies depending on the samples with different concentrations of activator ( $Mn^{2+}$ ) and quencher ( $Fe^{2+}$ ), and site occupancy of the  $Mn^{2+}$  ion between two cation sites in dolomite structure. The facts suggest that the behavior of the emission intensity with changes in temperature is not explained on the basis of a temperature quenching theory based on an increase in the probability of non-radiative transition with the rise of temperature (Mott-Seitz model). Probably activator ( $Mn^{2+}$ ) concentration affects temperature quenching effect on CL of dolomite considerably.

## Cathodoluminescence of calcite decomposed from dolomite in high-temperature skarn

KUSANO, Nobuhiro<sup>1\*</sup> ; NISHIDO, Hirotsugu<sup>1</sup> ; INOUE, Koichi<sup>1</sup>

<sup>1</sup>Okayama University of Science

Purple luminescent calcite associated with periclase has been found from the high-temperature skarn in Kanehira mine located in the eastern part of Hiroshima Prefecture. Calcite usually emits red to orange in cathodoluminescence (CL), but scarcely purple to blue. In this study we have conducted to clarify the emission center related to purple luminescence by using CL spectral analysis and the origin of the calcite during skarn mineralization.

The specimens collected from the skarn zone in the limestone contacted with intrusive granodiorite in the outcrop of the pit-tunnel. The polished thin sections of the selected samples were employed for optical observation and CL measurements. Color CL images were obtained using a cold-cathode type Luminoscope with a cooled-CCD camera. CL spectroscopy was made by a SEM-CL system, which is comprised of SEM (JEOL: JSM-5410LV) combined with a grating monochromator (OXFORD: Mono CL2). The CL emitted from the samples was dispersed by a grating monochromator (1200 grooves/mm), and recorded by a photon counting method using a photomultiplier tube. All CL spectra were corrected for total instrumental response, which was determined using a calibrated standard lamp.

Color CL imaging reveals two types of CL emission, red and purple, in calcite closely associated with spotted periclase. The CL spectra of both calcite show a broad emission band at 620 nm in a red region, which is assigned to an impurity center derived from an activator of divalent Mn ion substituted for Ca, where the intensity of red CL is higher than that of purple CL. Furthermore, the calcite with purple calcite exhibits a broad emission band at 400-500 nm in a blue region, which might be related to a defect center such as "back-ground blue" found in low-Mn activated calcite.

The calcite with purple CL is accompanied by spotted periclase grains, which is usually found as a component of metamorphosed dolomitic limestone. If the hydrate condition would be presumed during its formation, periclase could easily hydrate and alter to brucite and other magnesium minerals by action of the humidity. According to the results of heating experiments of dolomite, dolomite decomposes to calcite and periclase at around 750 °C, whereas calcite causes its decarbonation above around 850 °C. It implies that the calcite with purple CL might be persisting after the decomposition of dolomite under a dry condition at relatively high-temperature near 800 °C, and leave the defects in the calcite structure during thermal decomposition of dolomite, which can be assigned to the component of an emission band in a blue region.

## Cathodoluminescence characterization of terrestrial and extraterrestrial enstatite

OHGO, Syuhei<sup>1\*</sup> ; MISHIMA, Maki<sup>1</sup> ; NISHIDO, Hirotsugu<sup>1</sup> ; NINAGAWA, Kiyotaka<sup>1</sup>

<sup>1</sup>Okayama University of Science

Enstatite occurred in meteorite shows various cathodoluminescence (CL) emissions, whereas CL emission in terrestrial enstatite has not been reported so far. We have confirmed several luminescent enstatite in terrestrial samples. In this study, we have conducted to clarify the luminescence centers of terrestrial enstatite and comparatively discuss the CL of terrestrial enstatite and extraterrestrial ones in enstatite chondrite (E-chondrite).

Three enstatite with CL emission from Morogoro, Tanzania and Chandrika, SriLanka were selected for CL measurements. The samples were fixed on a brass disk with low-luminescent epoxy resin, and polished with a diamond paste. The polished thin sections of E-chondrite (Dar al Gani 734 and Y-86004) and Aubrite (Al Haggounia 001) were employed for CL examination. Color CL images were obtained using a cold-cathode type Luminoscope with a cooled-CCD camera. CL spectroscopy was made by a SEM-CL system, which is comprised of SEM (JEOL: JSM-5410LV) combined with a grating monochromator (OXFORD: Mono CL2). The CL emitted from the samples was dispersed by a grating (1200 grooves/mm), and recorded by a photon counting method using a photomultiplier tube. All CL spectra were corrected for total instrumental response, which was determined using a calibrated standard lamp.

Color CL imaging reveals various types of CL emissions, red, blue and purple in the both of terrestrial and extraterrestrial samples. The CL spectra of these enstatite show a broad emission band at 670 nm in a red region, which is assigned to an impurity center derived from activated divalent Mn ion substituted for Mg, and a broad emission band at around 400 nm in a blue region, which might be related to a defect center such as "intrinsic defect center" possibly raised during crystal growth.

CL spectra corrected for total instrumental response were converted into energy units for spectral deconvolution using a Gaussian curve fitting, because Gaussian curve in energy units can be assigned to one specific type of emission center (Stevens-Kalceff, 2009). The deconvoluted components can be assigned to the emission centers related to impurity centers of trivalent Cr ion (1.71 eV) and divalent Mn ion (1.87 eV) and to defect centers (3.18 eV). Furthermore, enstatite in Y-86004 E-chondrite gives additional emission component (3.87 eV) in a blue to UV region, which might be characteristic of the enstatite formed under the condition of low-oxygen partial pressure.

## Cathodoluminescence study of metasomatic feldspar in aegirine syenite from Iwaki Island, Ehime Prefecture

MAKI, Seiya<sup>1\*</sup> ; NISHIDO, Hirotugu<sup>1</sup> ; KAYAMA, Masahiro<sup>2</sup>

<sup>1</sup>Okayama University of Science, <sup>2</sup>Hiroshima University

In Iwaki Island, aegirine syenite was emplaced in the Ryoke granite during late Cretaceous time by alkali-rich hydrothermal metasomatism. The syenite and related rocks show various types of petrographic textures in response to the process of hydrothermal alteration, e.g. feldspar minerals. Feldspar exhibits a variety of cathodoluminescence (CL) colors depending on kinds of impurity elements and their concentrations, and defect densities related to Si-Al ordering and other structural disorder. Recently, the deconvolution method of CL spectra enables to assign the luminescence centers characteristic of the feldspar with satisfactory reliability (Kayama et al., 2010). In this study, we have conducted to clarify the metasomatic process through granite to syenite by CL spectral analyses for various types of feldspar.

Polished thin sections of the rock samples collected from granite, altered granite and syenite were employed for petrographic observations under a polarizing light microscope, CL measurements, and electron microprobe analyses (EPMA). Color CL images were obtained using a cold-cathode type Luminoscope with a cooled-CCD camera. CL spectroscopy was made by a SEM-CL system, which is comprised of SEM (JEOL: JSM-5410LV) combined with a grating (OXFORD: Mono CL2). The CL emitted from the samples was dispersed by a grating monochromator (1200 grooves/mm), and recorded by a photon counting method using a photomultiplier tube. All CL spectra were corrected for total instrumental response, which was determined using a calibrated standard lamp.

The feldspar in the unaltered granite shows apple green and blue CL emissions. The former is identified to plagioclase (Ab80, An20) characterized by divalent Mn activator at 556 nm, and the latter to alkali feldspar (Or90, Ab10) by defect center at 417 nm related to Al-O-Al. Altered granite has albite with red CL emission at around 750 nm, and alkali feldspar with inhomogeneous color of red to violet-blue emissions at around 400 nm and 720 nm. These CL emissions in a red region can be assigned to trivalent Fe activator in tetrahedral sites. The feldspar in syenite are mostly altered to albite with enhanced red emission at 748 nm, but minor alkali feldspar as residual after hydrothermal alteration exhibits dull red emission at 722 nm. The results of the spectral deconvolution reveals oxygen defect centers associated with Al-O-Al and Al-O-Ti bridges and impurity centers of trivalent Fe ions substituted for tetrahedral Al sites according to Kayama et al. (2010). Kayama et al. (2010) investigated the peak changes of a blue emission peak at 420 nm in alkali feldspar and they found that the elimination of Al-O-Al defect center was affected by hydrothermal metasomatism possibly at 250 °C. Therefore, the disappearance of blue emission in alkali feldspar in syenite implies that alkali-rich (sodium-rich) hydrothermal metasomatism for the formation of syenite could act at relatively high temperature above 250 °C successively after granitic magmatism.

## Provenance study of quartz grains in aeolian desert sediments using cathodoluminescence method

MASUDA, Risa<sup>1\*</sup> ; SANEYOSHI, Mototaka<sup>1</sup> ; NISHIDO, Hirotsugu<sup>1</sup> ; TSOGTBAATAR, K.<sup>2</sup> ; CHINZORIG, T.<sup>2</sup> ; MAINBAYAR, B.<sup>2</sup>

<sup>1</sup>Okayama University of Science, <sup>2</sup>Mongolian Academy of Sciences, Mongolia

Cathodoluminescence (CL), the emission of light caused by electron irradiation, has been widely applied in earth science, most extensively used in sedimentology. In such studies CL has the advantage that it can reveal characteristics which are invisible using transmitted light, e.g. growth zones of the crystals such as silica and carbonate minerals. In the case of quartz, its CL spectral feature is so complicated to be simply used for the identification of the provenance due to many emission centers related to various types of structural defects. In this study, we have conducted to clarify the luminescence centers in quartz selected from desert sediments using SEM-CL and evaluate quantitative ratios of the emission components of the CL spectra by the deconvolution method.

The quartz grains (#60-80 mesh size) in the aeolian sediments collected from Djadokhta formation (upper Cretaceous) in the Gobi desert were fixed on the slide glass with low-luminescent epoxy resin, of which surfaces were polished with 1 micron diamond paste. Color CL images were obtained using a cold-cathode type Luminoscope with a cooled-CCD camera. CL spectroscopy was made by a SEM-CL system, which is comprised of SEM (JEOL: JSM-5410LV) combined with a grating monochromator (OXFORD: Mono CL2). The CL emitted from the samples was dispersed by a grating monochromator (1200 grooves/mm), and recorded by a photon counting method using a photomultiplier tube. All CL spectra were corrected for total instrumental response, which was determined using a calibrated standard lamp.

All samples show dark blue CL emission, and exhibit two broad bands at 400 nm in a blue region and at 600-650 nm in a red region. CL spectra corrected for total instrumental response were converted into energy units for spectral deconvolution using a Gaussian curve fitting, because Gaussian curve in energy units can be assigned to one specific type of emission center (Stevens-Kalceff, 2009). The deconvoluted components can be assigned to the emission centers related to trivalent Fe at 1.65 eV, NBOHC at 1.89 eV, tetravalent Ti at 2.75 eV and trivalent Al at 3.19 eV by referring to Stevens-Kalceff (2009). We employed 10 grains randomly selected from collected 80 grains for each sample, and determined quantitative ratios of the emission components for these quartz grains using their integral intensities. We discuss variations of characteristic components among the sediments based on the results by a statistical analysis.